CHEMICAL REVIEWS

REVIEW

pubs.acs.org/CR

Attaching Persistent Organic Free Radicals to Surfaces: How and Why

Marta Mas-Torrent,[*,†,‡] Núria Crivillers,[†,‡,§] Concepció Rovira,[†,‡] and Jaume Veciana[*,†,‡]

[†]Institut de Ciència de Materials de Barcelona (ICMAB-CSIC), Campus UAB, 08193 Bellaterra, Spain

[‡]Networking Research Center on Bioengineering, Biomaterials and Nanomedicine (CIBER-BBN), ICMAB-CSIC, 08193 Bellaterra, Spain

[§]ISIS—CNRS 7006, Université de Strasbourg, 8 allée Gaspard Monge, 67000 Strasbourg, France

CONTENTS

1. INTRODUCTION

The grounds in molecular materials lie on using functional molecules as building blocks that self-assemble, following a bottom-up approach, into more complex structures that exhibit specific macroscopic properties, such as magnetic, optical, electrical, biological, or biomedical. For many years, scientists have been extensively investigating these molecular materials, motivated by their intrinsic properties as well as the possibility to tune them by molecular modification and solid-state design. In the latest years, though, this field has merged with another research area, surface engineering, and with this, a wide range of novel organic—inorganic hybrid materials have appeared, showing great potential for a vast amount of interdisciplinary applications.

Molecular surface engineering aims to design surfaces with specifically tailored properties through functionalization with appropriately chosen functional molecules. Bare substrates of metals and metal oxides tend to adsorb organic materials easily to lower the free energy of the interface between the substrates and the ambient environment. However, it should always be kept in mind that molecules at the surface of a material can exhibit different and unprecedented properties from those of the bulk ones, since they experience a completely different environment.[1] Molecules with a variety of functionalities have already been anchored on surfaces for the fabrication of chemical sensors,[2] for immobilizing biomolecules,[3] for tuning the surface wettability[4] and/or work function,[5] or for the preparation of surfaces with nonlinear optical properties.[6] Organic free radicals, which have been employed for a long time for preparing magnetic molecular materials,[7] are also exceptionally interesting molecules to functionalize substrates,[8] which is the focus of the present review.

An organic free radical is defined as a molecule with one or more unpaired electrons, and hence, it exhibits a magnetic moment. It is still generally believed that free radicals cannot be stable and isolable; however, a few families of stable and persistent radicals at ambient conditions have been around for many decades.[7b,9] Persistency of radicals is commonly related to a combination of odd electron stabilization by adjacent lone pairs or by delocalization and steric hindrance to prevent dimerization, hydrogen atom abstraction, or other undesired reactions. The interest they generate is not limited to the fabrication of magnetic materials but comprises a variety of areas.[9] Free radicals have been applied as reporter molecules to obtain structural, dynamic, or reactivity information from other systems (i.e., spin labeling, spin trapping, and ESR imaging). Further, radicals' reactivity has been exploited in catalysis or polymerization processes or for their ability to act as antioxidants. The redox character of organic radical-based polymers has also been exploited to develop batteries featuring fast electrode kinetics, reactant recyclability, and high redox capacity.[10] Another example of the potential of free radicals that is currently engendering great interest, particularly for applications in biomedicine, is in dynamic nuclear polarization (DNP), where an organic radical is used as polarizing agent to enhance NMR sensitivity.[11,12]

Inorganic—organic hybrid materials using persistent organic free radicals have also been reported. Thin films of stable radicals on a variety of substrates prepared by thermal evaporation in vacuum[13] or from solution, as for example by means of the Langmuir—Blodgett (LB) technique,[14] were described over 15 years ago.

Received: June 23, 2011
Published: December 21, 2011

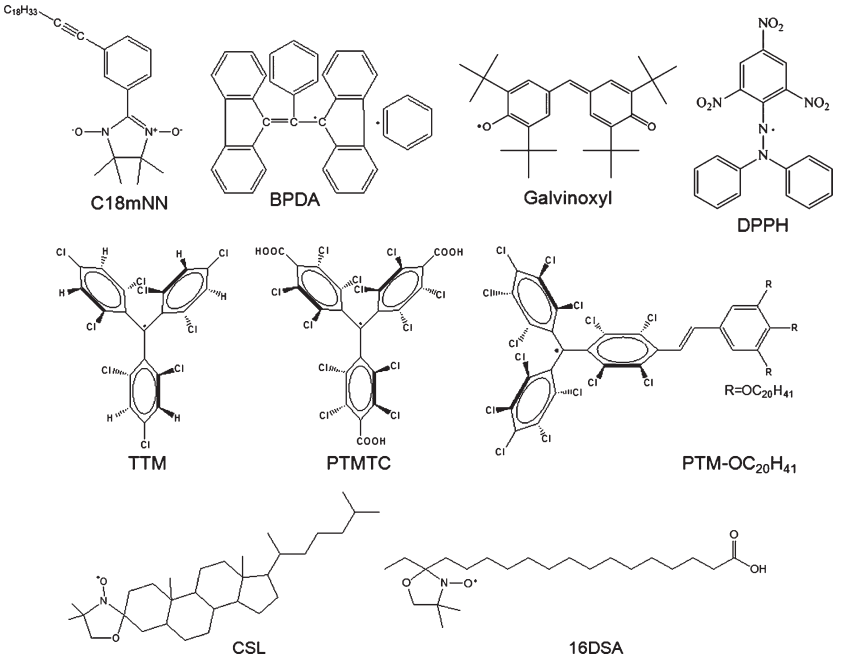

Figure 1. Molecular formulas of the free radicals studied physisorbed on a surface.

More recently, nanoscale patterns of persistent radical polymers on gold have been achieved by electrochemical oxidation with a conducting tip of an atomic force microscope (AFM).[15] Intercalation of free radicals into layered host matrices[16] or mesoporous materials[17] was also pursued. Also very recently, an elegant approach of growing inorganic−organic hybrid microcrystals by using nitroxyl radical exchange reactions was published.[18] However, the scope of this review is to overview the recent progress devoted to the organization of monolayers of these magnetic molecules on surfaces, paying particular attention to the preparation, characterization, and future perspectives of this novel-type of materials.

2. ORGANIZATION OF ORGANIC FREE RADICALS ON SOLID SUPPORTS

As for other organic molecules, the strategies followed to organize persistent organic radicals on surfaces can be generally divided into those using *physisorption* or *chemisorption* processes depending on the nature of the interactions between the substrate and the molecules. In the former process, the formation of the molecular assemblies is driven solely by weak intermolecular interactions, whereas, in the latter, strong chemical bonds, typically covalent, are established between the molecule and the substrate. In the following, a description of the molecular organization of organic free radicals obtained by physisorption and chemisorption will be carried out. Along this part, special attention will be paid to the intermolecular interactions as well as the interactions between the molecule and the surface that take place, since they are responsible for the preservation of the radical character and other physical properties of the molecule. Also, a brief overview at the end of this section of functionalized gold nanoparticles with radicals is included.

2.1. Organization of Organic Free Radicals on Surfaces by Physisorption

One of the first examples found in the literature of a radical surface monolayer was reported by Turek et al.[19] They prepared a single monolayer of an amphiphilic α-nitronyl nitroxyl radical (C18mNN, Figure 1) on silica plates by the LB technique as a first step toward the elaboration of a 3D supramolecular assembly of a magnetic material. By grazing incidence X-ray reflectivity, they found that the monolayer thickness was 22 $\pm$ 1 Å, with a roughness of 3.5 Å. This could be explained by a molecular configuration in which the molecules were standing on the surface in a brushlike fashion, with the α-nitronyl nitroxyl moiety directly interacting with the hydrophilic substrate and the aliphatic tails extending away and tilted. In such a 2D assembly, ferromagnetic interactions were evidenced (see section 3), demonstrating that the LB technique allows for some control of the intermolecular interactions on the surface through control of the molecular architecture.

An investigation regarding the influence of the substrate and methods employed for depositing by physisorption the free organic radical α,γ-bisdiphenylene-β-phenyallyl:benzene (BDPA, Figure 1) on the surface molecular orientation was carried out.[20] BDPA was evaporated under high vacuum as well as ultrahigh vacuum (UHV) conditions on highly oriented pyrolitic graphite (HOPG) and on Au(111), respectively, to prepare films with submonolayer thicknesses. It was found that the molecules on HOPG tend to aggregate together forming islands ranging in size from around a few nanometers to a micrometer, with a tendency to decorate the edges (Figure 2a). The molecules appeared to be mobile on the surface and diffused until they either settled down along the step edges or attached to other molecules. This mobility prevented the attempts to perform scanning tunneling microscopy (STM) imaging. On the other hand, monolayer-high islands of tens of nanometers in size (about ten times smaller than on graphite) were found on gold together with small clusters of a few molecules (Figure 2b). Interestingly, the molecules could be manipulated with the STM tip, since, in this case, the molecules did not diffuse much (i.e., the effective diffusion length was 10 nm on Au(111) and 500 nm on HOPG), and neither showed affinity to be on the terrace edges, demonstrating a greater surface−molecule

dx.doi.org/10.1021/cr200233g |*Chem. Rev.* 2012, 112, 2506–2527

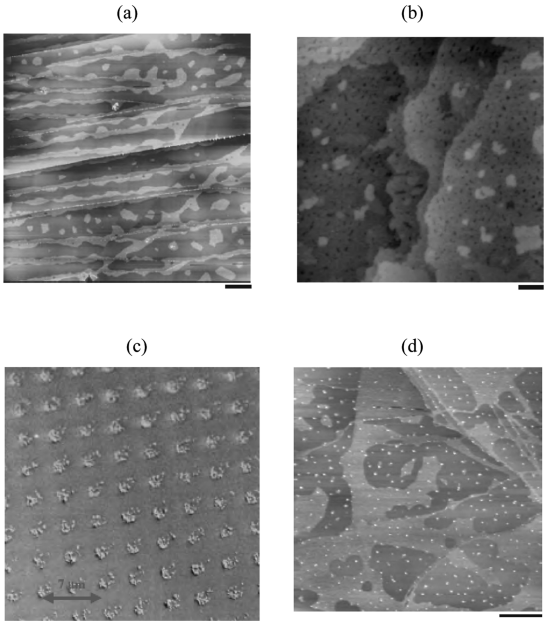

Figure 2. (a) AFM tapping mode image, 11 μm × 11 μm, on the monolayer of BDPA molecules evaporated onto HOPG. Scale bar = 1 μm. (b) STM image of BDPA islands on Au(111). 200 nm × 200 nm, I = 20 pA, V_{sample} = −850 mV. Scale bar = 20 nm. (c) The SEM image of the microcontact printed HOPG surface with an array of circles of BDPA molecules. (d) AFM tapping mode image on the BDPA islands deposited onto HOPG by solvent deposition, 6 μm × 6 μm. Scale bar = 1 μm. Reprinted with permission from ref 20. Copyright American Scientific Publishers 2006.

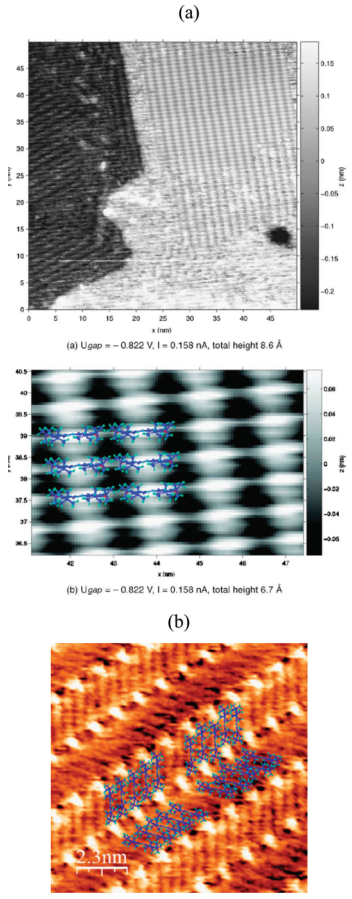

Figure 3. STM image and structure models for configuration I (a) and configuration II (b) of galvinoxyl monolayers sprayed on Au(111). Reprinted with permission from ref 23. Copyright American Physical Society 2006.

interaction stability. This was further elucidated by the STM imaging performed after two months of sample preparation. For both substrates, the thickness of the islands was found to be around 0.4 nm, much lower than the nominal height of the BDPA molecules (0.88 nm). This was attributed to the fact that the molecules undergo a conformational change while sitting on the surface, since one of the atomic planes of the molecule is rotatable and, thus, the actual molecular height depends on the molecule−substrate interaction.

BDPA was also physisorbed on HOPG using solution-based techniques such as microcontact printing and solvent deposition (i.e., drop casting and spin coating). Microcontact printing (μCP)[21] involves the inking of an elastomeric stamp, typically poly(dimethylsiloxane) (PDMS), with the molecules, and subsequently, by placing it into contact with a substrate, the ink molecules are transferred from the stamp to the substrate in the regions of contact. In a large HOPG area of 4 × 4 mm^2, an array of BDPA molecules was prepared using a stamp with circles of 1 μm of diameter and 4 μm space (Figure 2c). However, the thickness of such circles was around 6.89 nm higher than what was expected for a monolayer, indicating that the molecules aggregate and form clusters in solution rather than wetting the surface to form a monolayer, probably due to the high hydrophobicity of graphite. Finally, using solvent deposition in ethanol, similar molecular monolayers as the ones observed by vacuum evaporation were observed, but also some aggregates were found here which were attributed to a Stranski−Krastanov growth (*i.e.* monolayer followed by 3D crystal growth) (Figure 2d). All this work clearly shows the significant influence of the deposition method and the surface nature on the molecular organization of a free radical, which is driven by the molecule−molecule and molecule−substrate interactions on the surface self-assembly.

Galvinoxyl radical (Figure 1), which is known to be a very reliable radical scavenger,[22] has also been deposited on gold.[23] The sample preparation involved the spraying of a solution with a concentration range between 0.2 and 1 mM in ethanol directly into the vacuum chamber onto the atomically flat Au(111) surface. Two types of organizations, I and II, were observed. Both of them consisted of arrays of stacked molecules that followed the 6-fold symmetry of Au(111) and only differed in the angles between the molecules of adjacent stacks. The molecules were found to be standing upright on the surface, stabilized by $\pi-\pi$ overlap and hydrogen bonding interactions. In organization I, a line pattern with a periodicity of 15 Å was observed with a few etching holes. At room temperature, the holes were mobile until the system stabilized. The stacking distance was found to be 7 ± 0.7 Å. At 140 K, the same STM topography was observed, and the monolayer became more stable, staying at the same condition for several weeks. Figure 3a shows an STM image of this molecular organization with a possible model superimposed. Organization II was only observed after cooling the sample down to 40 K, although it was then preserved when warmed up. This result provides evidence about the competition between the kinetically and thermodynamically controlled organizations of the radicals deposited on a surface. In Figure 3b, the

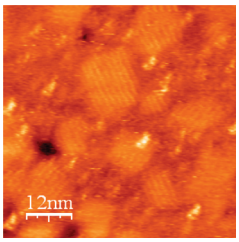

Figure 4. STM image (60 nm × 60 nm) of TTM molecules self-assembled on Au(111). Tip sample bias 0.3 V and tunneling current 15 pA. Reprinted with permission from ref 25. Copyright Elsevier Science BV 2009.

latter molecular configuration is shown with two possible pattern models: one with the molecules parallel inside the stack and another one with alternating shifts along the lateral axis of the molecule. The distance between molecules of one stack decreased down to 5.4 ± 1 Å in this second configuration, which could be due to the factor of 10 between the expansion coefficients of the gold surface and the galvinoxyl molecules.

Self-assembled monolayers of nitroxyl radicals such as 16DSA and CSL (Figure 1) were also obtained by physisorption on HOPG (0001).[24] In the first case, the measurements were performed at the liquid−solid interface, and it was found that the molecules form a highly ordered monolayer with domains that range from 10 nm up to 100 nm in size. On the other hand, the assembly of CSL on HOPG was carried out under UHV and revealed a well-ordered monolayer but without a domain structure.

Another family of persistent free radicals with a completely different nature that has been explored physisorbed on a surface is that of the polychlorotriphenylmethyl (PTM) radical. The tris(2,4,6-trichlorophenyl) methyl radical (TTM, Figure 1) was chosen as model compound to address the magnetic behavior of a metal surface after physisorption of this derivative.[25] The samples were prepared using the dip and rinse procedure,[26] which consists in immersing an annealed and clean gold substrate into a 10^{-3} M solution of TTM in dichloromethane for 30 s and, subsequently, rinsing it with pure solvent and drying it under nitrogen. As confirmed by STM, the TTM molecules were adsorbed on the entire gold surface and formed aggregates of a few molecules (diameter of less than 8 nm). After leaving the sample inside the STM chamber under nitrogen flow for a few hours, ordered domains of periodic rows separated by 1.5 ± 0.1 nm could be observed (Figure 4). The periodicity and dimensions of the rows were consistent with the molecular size of TTM molecules.

The PTM derivative PTMTC (Figure 1) has also been deposited on Au(111) by UHV evaporation and studied at submolecular resolution.[27] This PTM analogue has three carboxylic groups attached to the perchlorinated trityl skeleton that are known to drive the formation in the solid state of a layered hydrogen bonded open framework.[28] Two types of hydrogen bonded supramolecular assemblies of physisorbed PTMTC molecules were observed by STM after annealing the sample at 325−350 K. It is interesting to note that in both cases the surface assemblies were different from the one obtained within the layers of molecules in PTMTC single crystals, suggesting that, in the absence of interlayer PTMTC−PTMTC interactions, alternative 2D orderings of PTMTC molecules are energetically preferred in this 2D driven organization. The first arrangement followed a hexagonal pattern with an intermolecular distance

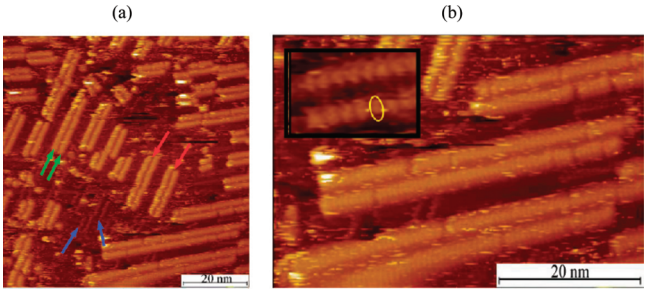

Figure 5. (a) STM image of PTM-$OC_{20}H_{41}$ from 1-phenyloctane on HOPG. I = 0.023 nA, V = −1.0 V. Green and red arrows indicate the separation between two adjacent rows and between two adjacent double rows, respectively, and blue arrows indicate some double rows from the first bottom-layer. (b) Zoom images show the stacked disklike bright features (highlighted in yellow) which form the rows. Reprinted with permission from ref 29. Copyright American Chemical Society 2009.

of ca. 1.13 nm. The second hydrogen bonded assembly shows a more densely packed assembly based on a unit cell (2 nm × 1.8 nm) of 4 PTMTC molecules, each bound to the closest one by hydrogen bonds. Here, it was also possible to image the helicity of each single molecule that results from the typical propeller-like conformation of PTM radicals. Indeed, alternating *Minus* and *Plus* helicity structures were seen, hence respecting the racemic composition when the PTMTC molecules are surface confined.

The self-assembly of a PTM derivative bearing long alky chains (PTM-$OC_{20}H_{41}$, Figure 1) on graphite has also been studied.[29] Taking into account the propeller-like conformation and bulkiness of the PTM moiety and that previous works had shown that in bulky systems similar to C_{60} it is necessary to have more than one long alkyl chain to ensure the adsorption of the molecules on graphite,[30] a PTM derivative bearing three long alkyl chains was synthesized. The self-assembly of this PTM radical was investigated physisorbed on graphite at the liquid−solid interface by STM, since in this environment the molecules can form the thermodynamically most stable supramolecular structures.[31] The molecules assembled spontaneously and formed ordered nanostructures at the interface, as illustrated in Figure 5. The bright areas in the STM images were attributed to the bulky and conductive PTM radical moieties in which their singly occupied molecular orbitals (SOMO) seem to favor electron tunneling. The molecules assembled into characteristic double rows with a separation of 2.2 ± 0.2 nm (green arrows in Figure 5) that corresponded to the formation of head-to-head PTM dimers favored by Cl···Cl interactions[32] that stacked maximizing the van der Waals interactions among adjacent alkyl chains. The distance between double rows was 8.0 ± 0.2 nm (red arrows in Figure 5), which is in agreement with the size of two extended molecules exhibiting enhanced CH−π interactions between the alkyl chains and the graphite lattice. Interestingly, the observed directions of the double rows in contact with the HOPG were restricted only to three directions with an angle close to 120°, suggesting that the molecules interact with HOPG, and therefore, the substrate symmetry strongly affects the growth direction of the rows. In this system, the long alkyl chains have two main effects: first they help to obtain well-ordered spin-containing two-leg ladders with a specific space between them, and second, they act as diamagnetic barriers between

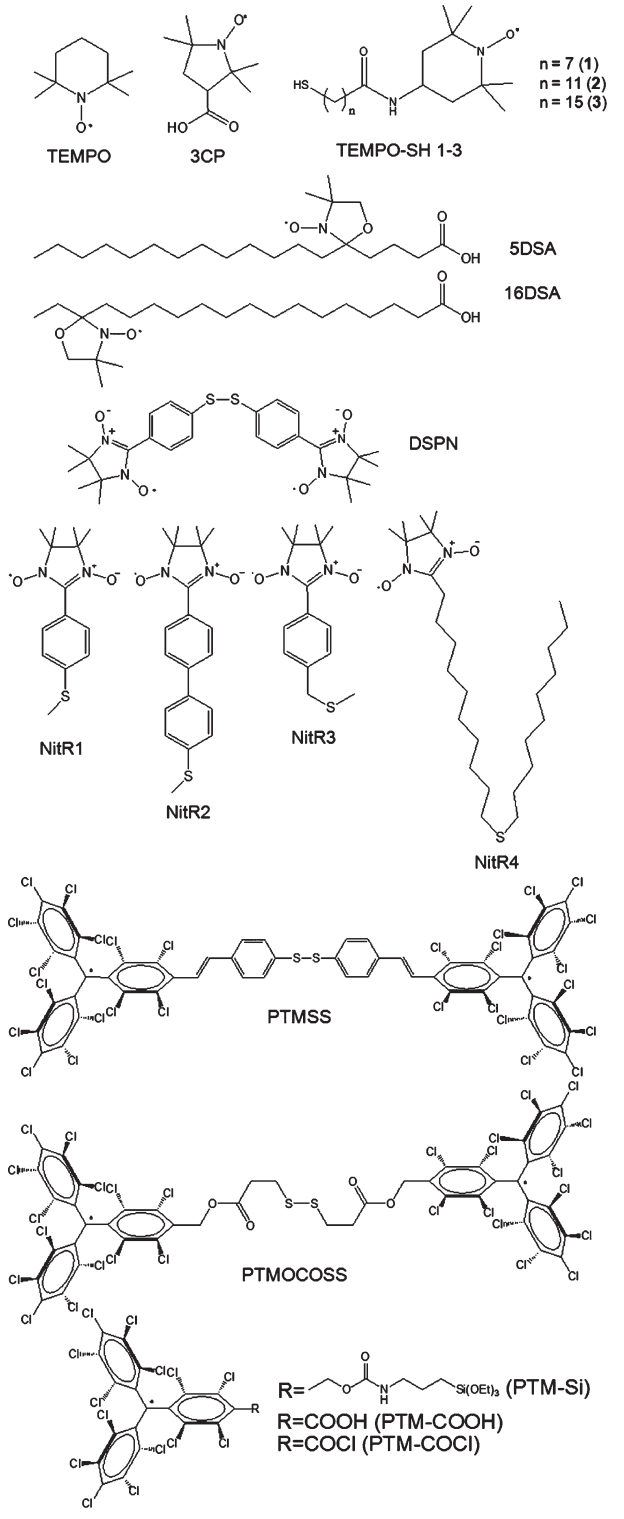

Figure 6. Molecular formulas of the free radicals studied chemisorbed on a surface.

neighboring radical units. Further, it was confirmed that the molecular organization previously observed in the liquid−solid interface was maintained after the solvent evaporation, which is attractive for future studies. Undoubtedly, such a spin-ladder type topology[33] offers new perspectives to design promising magnetic molecular architectures.

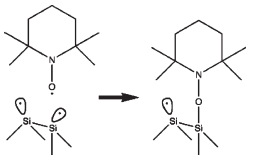

Figure 7. Schematic of a TEMPO radical reacting with one of the Si dimer dangling bonds on a clean Si(100) surface. Reprinted with permission from ref 35a. Copyright Elsevier BV 2004.

2.2. Organization of Organic Free Radicals on Surfaces by Chemisorption

Mainly organic radicals of the family of nitroxyls and α-nitronyl nitroxyls as well as PTMs have been chemically anchored on a variety of surfaces that range from metals (i.e., Au, Cu), inorganic semiconductors (i.e., GaAs, Si), metal oxides (i.e., ITO), or silicon-based oxides (*i.e.* quartz, glass, SiO_2). However, one of the earliest examples found is related to the generation of cyclopentadienyl radical ($^{\bullet}C_5H_5$, Cp) on Ag(100).[34] The samples were prepared by thermally desorbing previously physisorbed ferrocene $[Fe(C_5H_5)_2]$ molecules from the sample surface. Upon heating, most ferrocene molecules desorb intact while some undergo metal−ligand bond dissociation, leaving Cp radicals attached on the Ag surface. The unexpected low mobility found for Cp radicals on Ag(100) at room temperature was attributed to their strong bonding to the substrate. The energy loss spectroscopy data pointed out that the Cp−Ag bonding was more ionic in character than π-covalent. Furthermore, the authors demonstrated that these radicals could be manipulated and associatively desorbed with the STM tip at room temperature.[34]

The 2,2,6,6-tetramethyl-1-piperidinyloxyl radical, widely known as TEMPO (Figure 6), is a stable nitroxyl free radical that has an unpaired valence electron localized at the N−O atoms. TEMPO was investigated on Si(111) by UHV-STM.[35] This free radical was found to bind via its unpaired electron associated with the singly occupied molecular orbital (SOMO) to silicon, dangling bonds from the surface as illustrated in Figure 7. Although the radical character of the molecule was lost here, the formation of such a Si−O bond was proposed to be useful as an alternative route to graft molecules on a silicon surface. This silicon dangling bond−TEMPO reaction has already been applied for controlling the passivation of silicon surfaces,[36] growing molecular nanostructures on Si,[37] or for performing molecular electron transport studies.[38−40]

On the other hand, the radical 2,2,5,5-tetramethyl-3-carboxypyrrolidine nitroxyl (3CP, Figure 6) was deposited on Cu(110) by vacuum sublimation.[41] This radical was designed in order to anchor the molecule robustly to the surface involving the acid group, taking into account the affinity of this chemical group to copper. This reduces the possible interaction between the N−O and the surface and, therefore, enhances the possibility of preserving the unpaired spin. The STM images at 300 K at different coverage showed that from the very beginning the molecules tend to organize into 2D aggregates, as observed in Figure 8, where the discrete bright spots in the STM images with a diameter of 6−7 Å correspond to the 3CP molecules. The lower molecular mobility at room temperature confirmed the robustness of the assembly. Information regarding the bonding and molecular orientation at the surface was extracted from a combination of the STM experiments with reflection absorption infrared spectroscopy and DFT calculations. It was found that

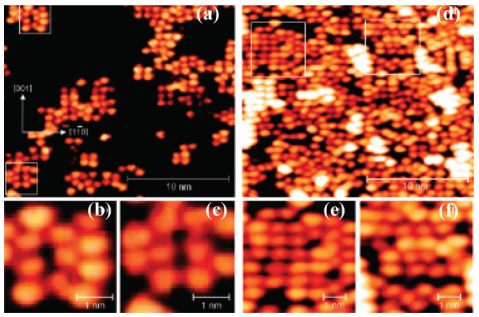

Figure 8. STM images of 3CP radical adsorbed on Cu(110) at 300 K recorded for low (a−c) and high (d−f) coverage. Reprinted with permission from ref 41. Copyright 2009 American Chemical Society.

the molecular structure played a critical role in the stabilization of the radical on the surface. Two Cu−O bonds between the carboxylate groups and specific short-bridge adsorption sites on Cu(110) were formed. In addition, this bonding together with the methyl substituents at the rings forces the molecule to be held upright with respect to the surface, preventing electronic overlaps between the Cu atoms and the NO groups, which could pair up, transfer, or delocalize the unpaired spin of the radical.

The most well-known example of a molecule grafted to a substrate is that of sulfur-containing self-assembled monolayers (SAMs) on gold, which were first described by Nuzzo and Allara in 1983.[42] Following this strategy, nitroxyl derivatives TEMPO-SH 1−3 (Figure 6) bearing a thiol functionality and an alkyl chain with different lengths were synthesized by coupling 4-amino TEMPO to the corresponding ω-thioacetyl carboxylic acids and subsequent deprotection of the thioacetates to thiols.[43] These materials were successfully used to functionalize gold substrates. The kinetics of this process was investigated using a quartz crystal microbalance, and it was established that the process was chain-length dependent: the rate increased with the molecular length. With a similar methodology, 4-aminoTEMPO was also grafted on gold, but the molecule reacted here with an already formed alkanethiol SAM with pendant acid groups.[44] Gold has also been modified with TEMPO following a different strategy. The 2,2,6,6-tetramethylpiperidine, known as TMP, was oxidized to TEMPO in a solution, which adsorbed on Au in the form of ammonium cation. Such a species at the potential of 0.5 V formed a permanent complex of gold and the nitroxyl radical.[45]

Moving again to a semiconducting surface, there is a current interest in functionalizing GaAs with organic molecules in order to chemically stabilize its inherently chemically unstable surface and to control the electronic properties of the resulting devices. In order to gain insights into the GaAs molecular functionalization, spin-labeled organic monolayers were fabricated.[46] The chosen molecules were 5-doxyl stearic acid (5DSA) and 16-doxyl stearic acid (16DSA), which, as in the previous example, bear a carboxylic acid anchoring group, and close or far away from it, respectively, a nitroxyl radical center is introduced (Figure 6). The samples were prepared by immersing the cleaned and etched substrates in 3 mM solutions of the molecules in ethanol overnight and, afterward, washing the samples with hexane. The ratio between the coverage of 16DSA to 5DSA estimated by infrared spectroscopy (IR) was 1.5 ± 0.2, which stems from the different locations of the nitroxyl moiety. In SAMs of 5DSA, since the bulky nitroxyl group is close to the surface, it does not allow a closer packing of the molecules, whereas in 16DSA, with the nitroxyl at the upper end, the long alky chains can organize, forming denser SAMs. Additionally, in the former case, the organization takes up to a week or two and, even after achieving a steady state, the layer is not well-ordered.

α-Nitronyl nitroxyl radicals have also been chemically immobilized on surfaces. Sugawara et al. reported the SAM formation and characterization of a bi(α-nitronylnitroxyl) biradical with a disulfide group linking the two radical centers (DSPN, Figure 6) on gold.[47] The substrate was soaked into an ethanol solution of DSPN, and the chemisorption process after the reductive cleavage of the disulfide group was traced by surface-plasmon resonance. It was observed that the chemisorption became complete after 20 min. The thickness of the monolayer measured by ellipsometry (12 ± 2 Å) was in agreement with the molecular length. This α-nitronyl nitroxyl derivative bears germinal dimethyl groups for kinetic stabilization, which could disturb the SAM formation. Nonetheless, by cyclic voltammetry (CV) experiments it was found that the SAMs were very dense, which was attributed to quadrupolar interaction among the highly polarized N−O groups.

Gatteschi et al. synthesized a series of α-nitronyl nitroxyls (NitR1−3, Figure 6) in which the chemical structure of the linker group was modified to evaluate this variation on the assembling process.[48] In all these analogues, a methylthio function was used to chemisorb on gold substrates to avoid the redox competition that could exist between the NitR radical and a thiol group, which is a more commonly used anchoring group to prepare SAMs on gold. STM characterization indicated that radicals NitR1 and NitR2 can bind to gold with two different orientations. However, thanks to the $-CH_2-$ spacer between the sulfur atom and the aromatic ring in NitR3, the degree of freedom of the molecules on the surface is reduced and, consequently, more ordered SAMs are formed. In addition, this chemical modification also stabilizes one molecular conformation which is more favorable for grafting, that is, one in which the methyl group is in a position closer to the methylenic spacer. On the other hand, substitution of the phenyl group with biphenyl did not lead to significant improvement of the ordering because, although $\pi-\pi$ interactions might be enhanced, also the degrees of freedom of the molecule increase. STM also proved only local ordering and that the radical molecules were quite mobile on the surface, probably due to the weak surface interaction provided by the methylthio group. Later on, the same group designed a α-nitronyl nitroxyl derivative (NitR4, Figure 6) with also a methylthio surface anchoring group and two long alkyl chains introduced to enhance the lateral packing of molecules in the SAM.[49]

An illustrative research work has been performed on PTM radicals chemisorbed on a variety of surfaces exploring different chemical bonding−substrate combinations.[50] For this purpose, two general approaches were followed: (i) a *direct anchoring* of the PTM radical on a surface with a covalent bond and (ii) a *two-step approach* consisting of growing a coupling SAM, which then interacts with the PTM derivative by the formation of either a covalent bond or a coordination bond or via electrostatic interactions (Figure 9).

For the *direct anchoring* strategy, the diradical PTMSS that incorporates a disulfide binding group to be anchored on gold was synthesized (Figure 6).[50b] This approach avoids the use of SH groups which are less stable in air for grafting the molecules to the surface and that can reduce the radical. In addition, it is worth noting that this derivative was designed so that in the resulting SAMs (**S1a**, Figure 10) the radical is fully conjugated and hybridized with the metallic gold surface. The preparation of SAM **S1a** was achieved by immersing a freshly cleaned gold

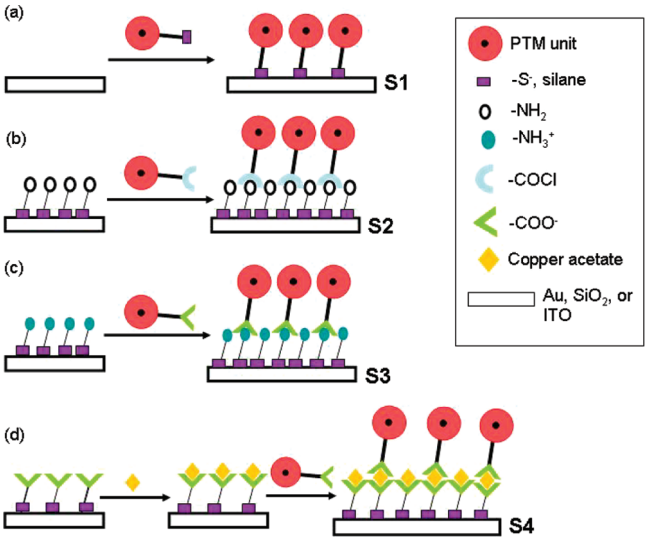

Figure 9. Scheme of the approaches employed to chemically anchor PTM radicals on a surface: (a) direct anchoring via a covalent bond; (b−d) two-step approach via the formation of a covalent bond (b), electrostatic interactions (c), or a coordination bond (d) with the coupling monolayer.

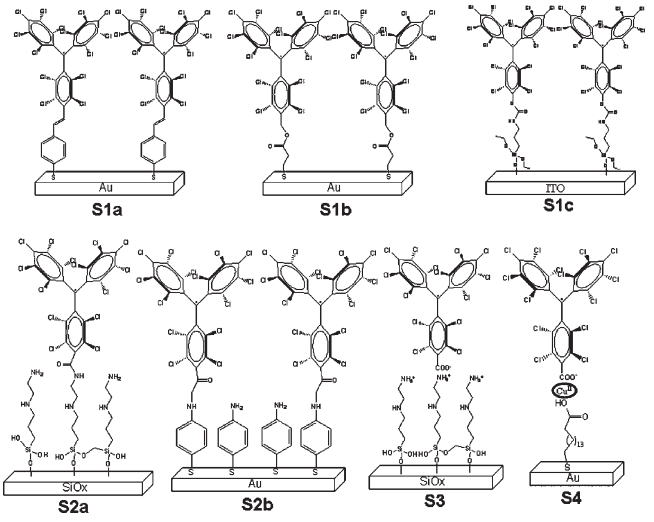

Figure 10. Chemisorbed SAMs prepared with PTM radicals.

substrate in a 10^{-4} M THF solution of PTMSS under argon atmosphere for at least 72 h in the dark (Figure 11, *path a*). After this time the monolayers were vigorously rinsed with abundant THF, to ensure that there was no physisorbed material on the substrate, and dried under a N_2 stream.

Interestingly, the same SAM was prepared using two additional approaches. The first one involved the functionalization of the substrate with a hydrogenated PTM precursor bearing a thioacetyl group (αH-PTM-SAc). Afterward, the SAM of αH-PTM-SAc was treated with a base (*i.e* a solution of tetrabutylamonium hydroxide in THF) for 24 h. This process induced a deprotonation reaction, in which the anchored αH-PTM groups were converted to the corresponding anions (Figure 11, *path b*). In the last route (Figure 11, *path c*), the SAM **S1a** is prepared by direct assembling of the anionic PTM species, which is generated from a solution of the αH-PTM-SAc analogue by addition of an excess of a strong base. In both cases, the anionic PTM SAMs

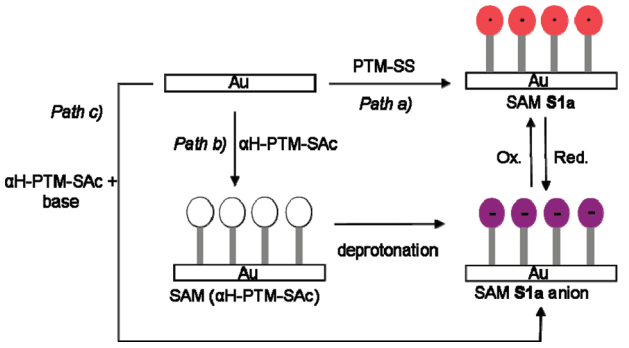

Figure 11. Routes followed to prepare PTM radical based SAM **S1a**. Reprinted with permission from ref 50b. Copyright American Chemical Society 2008.

were then oxidized to their PTM radical SAMs, either electrochemically or with a chemical oxidant. Although the direct anchoring of the PTMSS radical gave rise to higher surface coverage, this work elucidates the wide range of existing pathways to fabricate surface confined monolayers of redox active PTM organic radicals.

Alternatively, another more flexible and nonconjugated PTM diradical bearing a disulfide group (PTMOCOSS, Figure 6) has also been synthesized.[50f] Very dense SAMs of this derivative on gold were achieved by introducing the freshly cleaned substrates in a 10^{-3} M solution of PTMOCOSS in THF, in the dark, under argon and mild heating (30 °C) for the first 3 h, and at room temperature for the following 21 h (SAM **S1b**, Figure 10).

Within the direct anchoring strategy, but in order to functionalize indium tin oxide (ITO) substrates, a PTM radical with a terminal triethoxysilane moiety connected through a flexible chain (PTM-Si, Figure 6) was prepared. The corresponding SAMs (**S1c**) were prepared following a similar procedure as before, and they resulted in very dense and robust films, as explained in more detail in a following section.[50e]

As mentioned, the *two-step approach* consists in first functionalizing the surface with a coupling monolayer which bears a functional group able to chemically bind to the surface and a terminal chemical group that acts as a recognition site. Afterward, a functionalized PTM radical was immobilized on the substrate by forming either covalent, coordination, or electrostatic interactions with the first coupling SAM (Figure 9b−d). In order to graft the PTM derivative covalently within this strategy, SAMs of *N*-[3-(trimethoxysilyl)propyl]ethylenediamine on SiO_2 or 4-aminothiophenol on gold were prepared.[50a,c] The resulting substrates functionalized with the amino terminated monolayer were immersed in a solution of an acid chloride functionalized PTM radical (PTM-COCl, Figure 6), resulting in the formation of a covalent amide bond (**S2a** and **S2b**, respectively, Figure 10). The preparation of the PTM radical SAM solely via interlayer electrostatic interactions (**S3**) was similarly achieved on the SiO_2 based substrates.[50a] In this case, the amino group of the first monolayer was protonated by rinsing the sample with 4-morpholineethanesulfonic acid monohydrate buffer (pH 5.6), and subsequently, the substrate was immersed in a solution of a PTM radical with a carboxylic acid group (PTM-COOH, Figure 6) to form the ionic bond. The optical properties (absorption and fluorescence) of the SAMs prepared on quartz were successfully investigated. In addition, **S2a** and **S3** patterned surfaces were prepared by microcontact printing and visualized by laser scanning confocal microscopy or fluorescence microscopy due to the fluorescent nature of the PTM radical molecules.

dx.doi.org/10.1021/cr200233g |*Chem. Rev.* 2012, 112, 2506–2527

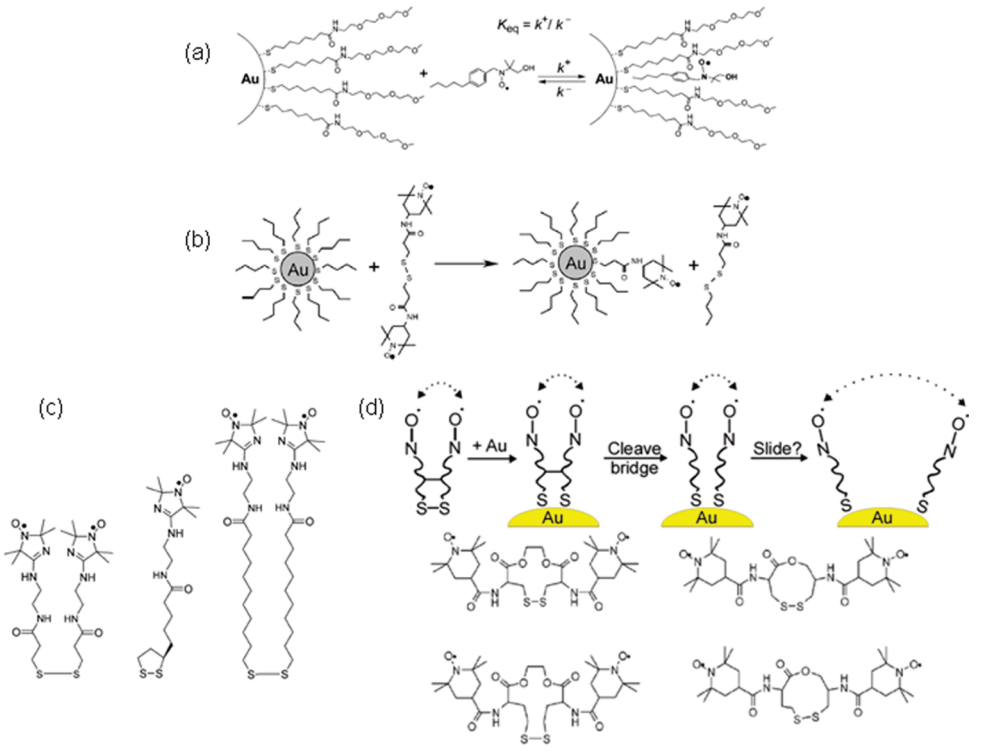

Figure 12. (a) Scheme of the inclusion of hydrophobic nitroxyl probes in the monolayer of a water-soluble protected gold cluster. Reprinted with permission from ref 53. Copyright 2004 American Chemical Society. (b) Preparation of spin-labeled gold nanoparticles by exchange reaction. Reprinted with permission from ref 55b. Copyright 2004 The Royal Society of Chemistry. (c) Structures of the series of spin-labeled disulfide ligands designed for anchoring to the gold NPs and being pH sensitive. Reprinted with permission from ref 55i. Copyright 2008 American Chemical Society. (d) Schematic drawing of the lateral diffusion of ligands on the surfaces of Au NPs and structures of the ligands used for the study. Reprinted with permission from ref 55g. Copyright 2008 American Chemical Society.

The grafting of a PTM derivative by means of a coordination bond with a metallic ion was achieved on a −COOH terminated SAM on gold following the layer-by-layer methodology, successfully reported for the growth of closed-shell planar molecules.[51] Two different approaches were used to validate the viability of this methodology.[50d] In the first one, a SAM of mercaptohexadecanoic acid (MHDA) on gold was immersed in a PTM-COOH/copper acetate 1/1 mixture, while in the second one the MHDA SAM was sequentially immersed first in a solution of $Cu(OAc)_2$ and, after rinsing and drying to remove physisorbed material, in a solution of PTM-COOH. Both strategies resulted in the surface grafting of the monocarboxy PTM derivative via the formation of a coordination complex where the Cu(II) metal ions act as linkers between the carboxylic groups of the MHDA SAM and the ones from the PTM-COOH (**S4**, Figure 10).

2.3. Organic Free Radicals on Nanoparticles

Besides the grafting to nominally *planar* surfaces, the unique and size-dependent optical, electronic, and catalytic properties of nanoparticles (NPs) make them an interesting solid support to investigate organic free radicals immobilized on their surfaces.

Up to now, most of the work done for grafting free radicals on NPs has been performed using gold NPs and substituted nitroxyls (Figure 12). There are three main strategies described to achieve the NP functionalization: (1) physisorption,[52] (2) inclusion of hydrophobic radicals into water-soluble monolayer-protected gold clusters (MPC),[53,54] and (3) chemisorption based on the same sulfur−gold chemistry employed for flat surfaces. The latter strategy was made following a ligand exchange reaction typically between the ligands of the functionalized NPs and free ligands in solution[55] but also between ligands of different nanoparticles (i.e., interparticle exchange).[56]

As an example, we describe the work done by Zhang et al. They prepared Au nanoparticles of two sizes, 15 and 2.5 nm, functionalized with the nitroxyl free radicals 4-R-2,2,6,6-tetramethylpiperidine, with R = -H (TEMPO), $-NH_2$ (TEMPAMINE), and -C═O (TEMPONE).[52] In particular, TEMPAMINE was chosen for the high affinity of the amine group to the gold surface. The physisorption of the three radical derivatives was demonstrated to take place since a significant reduction of the electron spin resonance (ESR) signal of the radical solutions in the presence of gold particles was observed. Moreover, the authors showed that a catalytic reaction in which TEMPAMINE is oxidized to TEMPONE occurred at the particle surface in the presence of oxygen in the solution, with the reaction being catalyzed by the gold particles.

As a summary, we can mention that the techniques employed to graft free radicals on surfaces have been the same ones as that utilized for other organic molecules. This demonstrates the high stability of organic free radicals during the deposition process and once immobilized on solid supports. A point worth mentioning about the molecular organizations achieved by chemically grafting free radicals to surfaces is the robustness of the resulting hybrid organic−inorganic materials, which is always superior to that of the assemblies obtained by physisorption. In contrast, except in very few particular cases, the lateral molecular order is poorer in the chemisorbed radical assemblies. Considering hence the easiness and versatility of the grafting techniques, the functionalization of surfaces

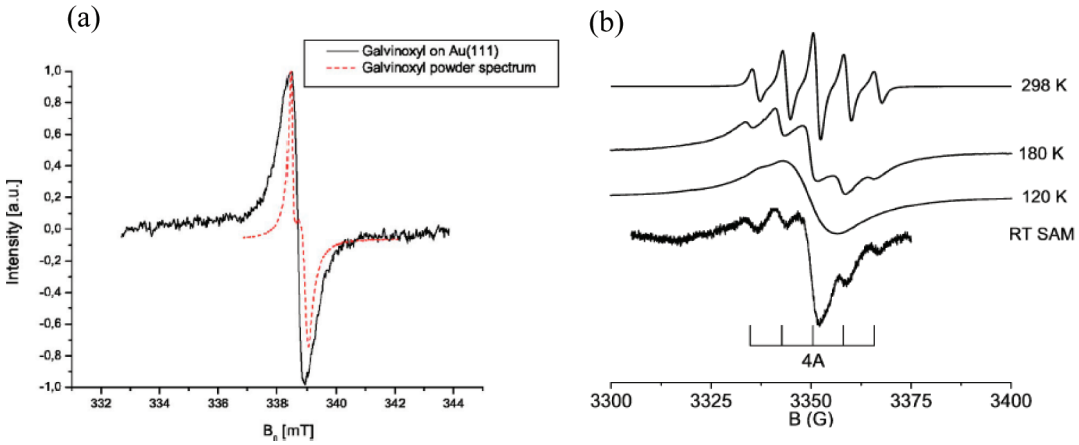

Figure 13. (a) ESR measurement of galvinoxyl on a Au(111) (black line) surface compared with the galvinoxyl powder spectrum (dashed red line). Reprinted with permission from ref 23. Copyright 2006 American Physical Society. (b) Temperature dependence of the ESR of NitR1 in solution compared to the room-temperature ESR spectrum of its SAM on gold. Reprinted with permission from ref 48. Copyright American Chemical Society 2007.

with properly and specifically designed organic free radicals opens wide perspectives for their applications. In addition, such hybrid inorganic−organic systems offer suitable platforms to study the influence of the surface on the paramagnetic species as well as the intermolecular interactions present between radicals.

3. ARE ORGANIC FREE RADICALS STILL PERSISTENT ON SURFACES? AND DO THEY KEEP THEIR PROPERTIES?

The first question that arises when an organic free radical is adsorbed or grafted on a surface is whether its magnetic nature given by the presence of the unpaired electron will persist. Indeed, the radical character of the molecules on a surface can be lost due to possible electron transfer to/from the substrate or to atom abstraction by the radical originated by specific electronic interaction with the surface. In this section we present an overview of the different techniques that have been used to detect and address organic radicals on surfaces, as well as how theoretical calculations help with gaining a better understanding of the adsorption mechanism and possible magnetic interactions.

3.1. Electron Spin Resonance (ESR)

The most commonly used magnetic technique for the detection of paramagnetic spin centers is ESR. It measures the energy absorption produced under microwave radiation by changes of the precession of an induced macroscopic magnetization around an external static magnetic field. This highly sensitive technique is widely used for characterizing organic free radicals in solution and in solid state, and it represents also a proper means to detect the spin signal when the radicals are deposited on a surface, allowing determination of whether the radical nature is preserved upon chemi- or physisorption on a specific substrate. In this regard, we find several examples in the literature where ESR has been used for this purpose. The largest amount of work relies mainly on the study of PTM,[29,50a,50b,50d,50e] α-nitronyl nitroxyls,[19,24,46−49] and other nitroxyl radicals, such as TEMPO and derivatives,[45,57] and galvinoxyl[23] deposited on surfaces. Below, some of these works are explained in more detail.

In 2002, Matsushita et al. demonstrated by ESR that the novel open-shell π-conjugated disulfide carrying an α-nitronyl nitroxyl group (DSPN) remained intact during the chemisorption process on gold.[47] This technique has also been employed for physisorbed layers, as it was demonstrated by Speller and coworkers for a layer of galvinoxyl radical on Au(111).[23] The corresponding ESR spectrum (shown in Figure 13a) confirmed that the radical is not reduced upon binding to the surface but persists as a free radical. The observed singlet line had a line width of 8.1 G, which exceeds the line width of the powder spectrum (red dotted line), in accordance with the higher intermolecular distance inside the molecular layer compared to that in the crystal. Mannini et al. performed a more extended study and used ESR to verify the effect of the deposition procedure on the magnetic properties of the series of the α-nitronyl nitroxyls NitR1−3 and to get information about the dynamics and the degree of organization of the deposited molecules (Figure 13b).[48] The hyperfine structure of the signal coming from the coupling of the unpaired electron with two equivalent ^{14}N nuclei undoubtedly confirmed the integrity of the NitRs molecules on the surface. ESR also allowed for the estimation of a complete coverage of the surface by comparing the signal with the one obtained from a NitR solution containing a known and comparable number of spins. The temperature and time evolution of the ESR spectrum of the SAM suggested quite a large mobility of the radical, in agreement with the STM results. Additionally, the absence of any angular dependence of the room-temperature ESR spectrum with the orientation of the sample with respect to the external magnetic field suggested a quasi-isotropic motion of the radicals anchored to the surface. Such fast motion must average the anisotropy of the g factor and the nuclear magnetic dipole hyperfine interaction (A) tensors that are strongly dependent on the molecular orientation. This molecular motion occurs on a time scale that is slow for the ESR spectroscopy but is fast and thus undetectable for STM, meaning that the small regions of local ordering observed and previously mentioned by STM do not sum to give a large-scale order. Such ordered domains could hence be formed as a consequence of different oriented domains of the gold substrate and roughness of the polycrystalline surface.

ESR investigations on the 16DSA and CSL radicals on HOPG were also performed, being especially relevant for the CSL, since during the film formation high temperatures are required that could destroy the paramagnetic character of the molecules. ESR data suggested a molecular immobilization and the formation of ordered

structures for the 16DSA upon adsorption, and in the case of the CSL, the ESR spectrum showed that the molecules were not reduced and retained their paramagnetic nature after the heating procedure.[24]

Importantly, as briefly introduced in the previous example, ESR is, in principle, a suitable technique to get structural, dynamic, and electronic information on organized organic radical monolayers, and in addition, it gives information on the interaction between the adsorbed molecules and between the molecule and the substrate.[58] For example, spin−spin interactions in magnetic LB films of organic free radicals have been studied by ESR. Zhu and co-workers[14c] prepared LB films based on a novel organic compound with two radical substituents, a α-nitronyl nitroxyl and α-imino nitroxyl, and a long hydrophobic chain. ESR spectra of the biradical deposited on quartz glass were measured at different angles (θ) between the direction of the magnetic field and the substrate surface and showed that the g factor decreased with decreasing values of θ. Moreover, a dependence of its ESR intensity (I) on the magnetic direction was also observed, suggesting an anisotropy in the magnetic behavior of the radicals forming the LB film. Interestingly, the temperature dependence of I further demonstrated antiferromagnetic interaction at low temperature which probably overshadows the expected intramolecular ferromagnetic interaction, observed for polycrystals of the same radical. On the contrary, as introduced in section 2.1, Turek et al.[19] reported antiferromagnetic interactions in the bulk material of C18mNN, while clear evidence of ferromagnetic interactions was observed in the temperature dependence of the ESR response of a single LB monolayer of this radical. The integrated intensity of the absorption line is known to be proportional to the static susceptibility χ, and hence, considering this, the authors found that the experimental data for the C18mNN monolayer fitted with a Curie−Weiss law with a positive Weiss constant. These magnetic interactions were attributed to the steering induced by the molecular organization in the monolayer. Moreover, the line width and g-factor anisotropy observed in the experiments, where the ESR signal was recorded in three orthogonal planes with respect to the LB film, allowed extraction of an overall picture of a 2D magnetic layer having its magnetic axis oriented along the normal to the substrate, *i.e.* along the long molecular axis.

ESR has also been successfully employed for characterizing other types of organic−inorganic hybrid materials in which other types of solid supports were used. As an example, an alkenylated TEMPO radical was grafted on a porous silicon (PS) surface and the ESR spectrum of the hybrid TEMPO-PS proved the covalent grafting and chemical integrity of the radical. It is known that a large electron dipole−dipole interaction, which is dependent on inter-radical distances, produces a fast relaxation of the electron spins and thus a broadening of the ESR lines. The lack of the linewidth enlargement expected for a densely packed 2D array of TEMPO molecules revealed a low coverage.[58] Furthermore, ESR recorded in the temperature range 20−370 K permitted study of the dynamics of the TEMPO radical molecules on the PS. The ESR spectrum of the TEMPO-PS at 220 K was characteristic of immobilized nitroxyls. However, the spectral features corresponding to the mobile nitroxyls were progressively more evidenced upon raising the temperature while the spectral component related to the immobilized nitroxyl decreased accordingly. The defined mobile fraction (mobile component/total intensity of ESR spectrum) was observed to contribute significantly to the ESR spectrum only at $T > 300$ K. With this observation, the authors concluded that the relatively low coverage and negligible chain-to-chain interaction imply that the temperature dependence of the chain mobility is mainly dominated by the internal conformation degree of freedom. At least two local conformational mobilities were assigned. Upon heating, the "rigid" molecular fraction converted into a mobile one, where the conformational freedom of the alkyl chain is comparable to what one can measure in liquid solution.

ESR has also been extensively employed for the characterization of the physical and chemical properties of gold nanoparticles when they act as a solid support for paramagnetic species, as well as to investigate the processes that occur on their surfaces.[59]

3.2. Single-Spin Sensitive Scanning Probe Microscopies: SP-STM and ESN-STM

Although relevant information can be obtained from the ESR studies, the very small amount of material in a single monolayer is a limitation, since it is close to or, in some cases, even lower than the sensitivity limit of the ESR. In addition, when analyzing radical monolayers attached to surfaces, one must be careful to avoid the presence of multilayers of the radicals, since the ESR response of these latter species may overlap with the signals (if any) produced by the radical monolayer in direct contact with the surfaces. In this line, we encounter two main drawbacks when facing the actual demand of scaling-down the detection limit: (1) the lack of spatial resolution and (2) the need for approximately $10^{10}-10^{12}$ spins on the sample for a detectable signal.[60] To overcome this problem, the combination of the subnanometer spatial resolution of the scanning probe microscopy (SPM) techniques with single-spin sensitivity has gained much attention in the last years, as it is suitable for the detection of free radical molecules, *i.e.* electron spins, at the atomic level. There are two main techniques used for the magnetic addressing of individual molecules: spin-polarized STM (SP-STM) and electron spin noise STM (ESN-STM).[8] The ideal situation for performing this type of experiments is when singly dispersed molecules or isolated small clusters of them are present on a surface, thus enabling probing of single molecules and, hence, single spins.[20]

SP-STM is a technique which is capable of mapping out the magnetic orientation of magnetic systems on a surface down to atomic scale. It uses a ferromagnetic tip to produce a spin-polarized tunneling transport which allows one to detect magnetized species.[61] The tunneling conductance is then a function of the relative orientation of the magnetic moments of the tip and the sample. Up to now, SP-STM has been mainly applied successfully to metal atoms and only recently have the first examples of SP-STM on magnetic molecules appeared.[62] The different spin tunneling measured in a single Co-phtalocyanine molecule depending if the spin of the molecule was oriented up or down demonstrates the potential of this technique.[62b] STM imaging of galvinoxyl radicals on Au(111) using in this case an antiferromagnetic MnNi tip was attempted.[23] Such an antiferromagnetic tip was chosen since it has no stray field that influences the sample magnetism. However, down to 140 K no appreciable differences in topography were found using these tips. This implied that either the sensitivity, i.e. the spin-polarization of the tip, was too low or the spin-ordering in the molecular aggregates was not sufficiently strong or even absent.

On the other hand, ESN-STM is based on the detection of spin noise (small signal) in the tunneling current of the STM experiment at a frequency corresponding to the electron Larmor frequency of the spin. Besides the use of this technique to detect dangling bonds at silicon surfaces as originally demonstrated,[63] the signal has also been detected for organic free radicals such as

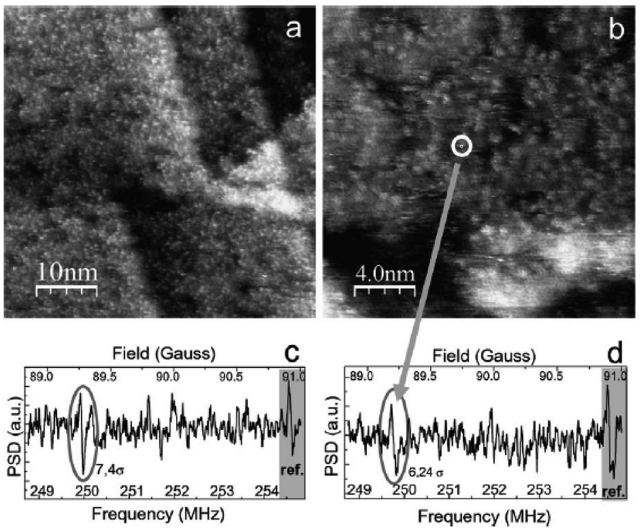

Figure 14. (a) STM image of NitR3 deposited on Au(111) during ESN-STM measurements. (b) STM image of NitR3 observed on a zoomed area. (c and d) ESN-STM spectra of a single NitR; signal evidenced by a circle. During the spectroscopy, bias voltage and tunneling current were, respectively, 0.1 V, 1 nA and 0.1 V, 0.1 nA. Reprinted with permission from ref 66. Copyright 2008 Elsevier.

DPPH (1,1-diphenyl-2-picrylhydrazyl),[64] TTM,[25] BDPA,[65] and NitR3 (Figure 14).[66]

As introduced above, the precise positioning of spin probes at the surfaces is crucial to further develop techniques such as SP-STM and ESN-STM. It is very important to prevent electron migration or lateral diffusion of the molecules during the experiment. Moreover, one has also to bear in mind that the presence of several paramagnetic radicals in the surrounding of the spin probe can alter the local magnetic field and the spin dynamics of the probe. In this regard, we find an interesting example reported by Messina and Fradin where they successfully inserted individual molecules and dimers of DPPH (Figure 1) into a diamagnetic conducting matrix.[67] In particular, they exploited the self-assembly of 1,10-phenanthroline on the Au(111) surface to host the paramagnetic molecules. The resulting modified surface was suited for subnanometer-scale STM investigations, where the authors found the right experimental conditions (solvent, concentration, annealing temperature, and sample time exposition) to intercalate the DPPH molecules into ordered and extended arrays of 1,10-phenanthroline. Importantly, this strategy is not restricted to DPPH but could be extended for a more general application.

In recent years, other more complex magnetic techniques have been used to detect the presence of small numbers of spins,[68] although they have not yet been applied to organic free radicals. Such techniques comprise optically detected magnetic resonance (ODMR), a superconducting quantum interference device (SQUID),[60] X-ray magnetic circular dichroism (XMCD) spectroscopy,[69] and magnetic resonance force microscopy (MRFM).[70] Further, studies on the Kondo effect resulting from the exchange interaction between the local magnetic moment in the molecule and the conducting electrons,[71] and depth-resolved β-detected NMR (β-NMR), where one measures the nuclear magnetic resonance and relaxation of ^{8}Li,[72] have also been performed.

3.3. Additional Nonmagnetic Techniques

Besides the magnetic techniques presented above, which can directly detect the spin of the radicals, giving a nonambiguous

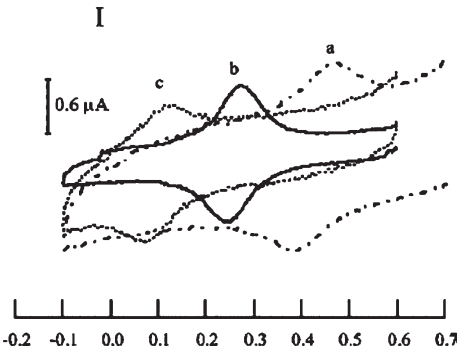

Figure 15. Cyclic voltammogram of a galvinoxyl-modified gold electrode in 0.1 M Na_2HPO_4 at pH (a) 4.6, (b) 7.8, and (c) 10.4. Reprinted with permission from ref 23. Copyright American Physical Society 2006.

evidence of the persistence of the paramagnetic character when the molecules are grafted on the surface, the intrinsic characteristic electronic properties of some of the organic radicals can also be exploited as a tool to further characterize and confirm the nature of the free radicals confined on the surface. Information related to the molecular electronic structure can be extracted by employing a variety of structural, electrochemical, or spectroscopy techniques.

For instance, near-edge X-ray absorption fine structure (NEXAFS) has been found to be a useful tool to verify the presence of radical species on the surfaces. This technique was used to characterize SAM **S4** (Figure 10) on the basis of monocarboxylic substituted PTM radicals grafted on top of a carboxylic-terminated SAM (MHDA-SAM) through a copper(II) linker.[50d] K-edge polarization dependence NEXAFS for the MHDA SAM showed the expected features C(C−H) → R*, the C(C═O) → π^*, and the C−C → σ^* resonances. After PTM deposition, four additional resonance peaks were observed (282.9, 285.4, 285.5, 286.6 eV), where the last two were assigned to the C(Ph) → π^* transition and the peak at 285.4 eV to the residual acetate groups coordinated to copper ions. The authors determined the peak at 282.9 eV to be a signature of the PTM radical. This peak located below the corresponding C 1s binding energy (284.9 eV) unequivocally revealed the presence of empty states with energy lower than the substrate Fermi level. Accordingly, this peak had to be assigned to an excitation of C 1s core−electrons in the half-filled highest occupied molecular orbital or singly occupied molecular orbital (SOMO) of the radical ligand. This observation further corroborated what was also observed by ESR for this monolayer, i.e. that the open-shell state of the molecule remained after grafting it to the surface.

Cyclic voltammetry (CV) has also been employed to determine the redox character of SAMs based on organic free radicals such as galvinoxyl,[23,73] PTM,[50b,c,e,f] and nitroxyls[43,44,74] on conducting surfaces (i.e., gold or ITO). The electroactivity in these species is intrinsic of their radical character due to the presence of the SOMO into which one electron can be added or extracted. In these experiments the substrate functionalized with the radical SAM is employed as a working electrode. Figure 15 shows the CV of a galvinoxyl-modified gold electrode.[23] The observation of the characteristic redox process of galvinoxyl evidences the persistence of the radical. The linear variation of the peak currents with scan rate and the small peak-to-peak separation are typical characteristics of electroactive surface confined species. Moreover, from the CV experiments it is possible to extract a qualitative value of the surface coverage. CV performed on gold and on ITO

covalently modified with PTM radicals (surfaces **S1a-c** and **S2b** from Figure 10) also showed their typical reversible redox response, ascribed to the reduction to the corresponding carbanion form, confirming thus the persistence of the radical species on the surface.[50b,c,e,f] Further, Levillain et al. have performed a careful study on the electrochemical characteristics of gold surfaces functionalized with SAMs based on TEMPO-SH 1−3 radicals (Figure 6) and mixed SAMs of these molecules with alkanethiols to study the distribution of electroactive centers on the surface as well as the ion-pairing formation.[74] Also, Finklea et al. have determined by electrochemical means the reorganization energies of $TEMPO^{\bullet}/TEMPO^{+}$,[44] which is of high interest due to the wide electrochemical applications of TEMPO and its redox partners.[75]

In addition, in the particular case of the PTM derivatives, the characteristic optical properties of the radical and its redox pair, the PTM anion, have been used to characterize PTM-functionalized SiO_x, ITO, and Au substrates, being as well a proof of the presence of the radical species on the surface.[50a,e,f] Indeed, PTM radicals have characteristic absorption bands centered around 385 and 570 nm, which are related to electronic transitions involving the SOMO molecular orbital, whereas PTM anions show only a broad and intense absorption band at 510 nm.

3.4. Theoretical Studies

In addition to the experimental tools, theoretical calculations have also been employed to gain in-depth understanding of the structure and magnetic properties of some radicals on the surface. Totti et al. performed density functional theory (DFT) calculations on 4-(methylthio) phenyl nitronyl nitroxyl (NitR1) and 4-(methylthio) methyl phenyl nitronyl nitroxyl (NitR3) on Au(111).[76] As a first step, the optimization of the unit cell was performed. On Au_{48} and Au_{54} systems they observed a chain-like disposition where the magnetically active nitroxyl groups were nearest along a certain direction. An interchain interaction for the possible magnetic properties of the monolayer was therefore expected leading to ladder-like, two-dimensional magnetic interactions. By the enthalpy energies of formation, the authors observed that $NitPhCH_2S^{\bullet}$ forms more stable monolayers than $NitPhS^{\bullet}$, in agreement with what was observed experimentally by STM, which was previously discussed (see section 2.2). For a preliminary insight into the magnetic properties, they performed B3LYP calculations on the optimized Au_{54}−$NitPhCH_2S$ geometry. The two magnetic couplings (J) expected for such a hybrid material, the intra (within the radical molecule) and inter (between two radical neighbors), were computed. The J inter coupling was calculated to be antiferromagnetic (132.3 cm^{-1}) for a dimeric unit with a closer radical−radical distance of 4.56 Å and ferromagnetic by −59.0 cm^{-1} on a different dimeric unit picked with a radical−radical distance of 8.14 Å. The authors claimed that for a quantitative conclusion about the J's values it requires calculations on larger model complexes. Recently, also Totti and co-workers reported on the use of periodic/molecular DFT calculations to study the energetics, structure, bonding, and magnetic exchange interaction of SAMs of the NitR1 and NitR3 thiolated radicals. In particular, they computed the spin density to determine its delocalization to the Au(111) (Figure 16).[77] The results showed that the gold atom with the shortest Au−S contact had a negative spin density, indicating a predominant spin polarization mechanism for the spin distribution to the Au(111), and that, for longer Au−S contacts, on the first layers all had positive spin density. The authors stated that the large computed exchange interaction indicates that the gold layer in fact acts as a superexchange medium and that the efficient spin delocalization on the gold layer can, therefore, be the reason for a stronger intermolecular coupling.

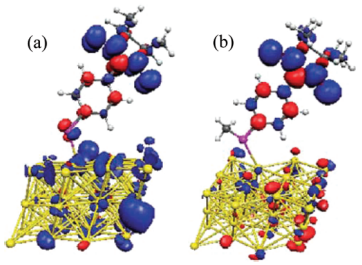

Figure 16. Computed spin density plots for two NitR1 forms on gold: (a) $^3NitR1\text{-}S^{\bullet}$, i.e., the triplet state formed when the unpaired electron on the S head resulting from the homolytic cleavage of the S−C bond can couple with the one delocalized on the N−O NitR orbitals, giving rise to triplet and singlet states, and (b) $NitR1\text{-}SCH_3$. The blue color represents positive spin density while the red represents negative spin densities. Reprinted with permission from ref 77. Copyright Royal Society of Chemistry 2010.

Computational modeling has been employed to investigate the binding of TEMPO to clean Si.[35a] TEMPO radical and Si clusters were constructed, with the optimized geometries being the following: $TEMPO\text{-}Si_9$, $TEMPO\text{-}Si_{48}$, $TEMPO\text{-}Si_9H_{12}$, and $TEMPO\text{-}Si_{48}H_{36}$. DFT calculations of the frontier orbitals (the SOMO of the molecule and the HOMO of the cluster) were performed. The interactions of these frontier orbitals, separated by a small energy difference (27 meV), could explain the apparent facile reaction between the nitroxyl radical and a Si dangling bond. Moreover, calculated state density isosurfaces over a range of occupied and unoccupied states for the $TEMPO\text{-}Si_{48}H_{36}$ cluster model agree qualitatively with the STM data, which indicates that TEMPO molecules exhibit a strong topographic bias dependence over a range of sample biases.

Marks et al. used DFT to investigate in detail the possible onward reactions of nitroxyl radicals bound to a silicon (001) surface.[78] The focus of this work was to reveal the conditions under which the nitroxyl N−O bond breaks and how the subsequent fragments react with the surface. The authors used the nitroxyl radical H_2NO as a simplistic system which then could serve as a model for larger radicals, such as TEMPO. They studied the dissociation of the N−O bond on three representative surface environments: a hydrogen-terminated surface with a single missing hydrogen defect, a clean surface with a single hydrogen forming a Si−Si−H hemihydride, and the clean surface with no hydrogen-termination. The main finding of this study was that the N−O bond in the nitroxyl radical rapidly dissociates on the silicon surface at room temperature when dangling bonds are available nearby. They compute the binding energy of the TEMPO on the surface, before and after dissociation, with the dissociated structure being 2.3 eV more stable than the adsorbed configuration and, hence, showing that the dissociation is an exothermic process. Their studies found the absence of room temperature dissociation on hydrogenated surfaces (missing hydrogen defect). This result was in agreement with previous experimental results where the TEMPO molecules could be placed in missing hydrogen defect sites and removed again.[36,37]

Theoretical studies using the hybrid DFT method to better understand the magnetic interactions between gold nanoparticles and stable organic radical species have been carried out.[79] To

do that, they examined small gold clusters, Au_3 and Au_{13}, and the SPN-hex π-radical as a hybrid model system. The SPN-hex radical is the monosulfide derivative of the DSPN (Figure 6) with a hexyl chain replacing one of the methyl groups. The results suggested that the correlation between the delocalized Au electrons and the localized spin moment on the organic radical through the medium of the spin polarization is important and the electron/hole doping into the Au−organic spin molecule hybrid system could change the magnetic interaction of the ground state.

The above presented results demonstrate that the radical character of stable organic radicals reported so far is persistent after physi- or chemisorption on a variety of substrates, with an exception being the cases where the unpaired electron takes part in the bond formation with the surface. These results are highly encouraging to further study the exciting properties that these materials exhibit, hence, opening the possibility to exploit them for a wide range of applications.

4. PERSPECTIVES OF ORGANIC FREE RADICALS ON SURFACES

As mentioned, in addition to the inherent magnetic properties that organic radicals exhibit, these materials are also promising to be applied in a large variety of fields. Similarly, the immobilization of radicals on surfaces by covalent bonds gives rise to novel and robust organic−inorganic hybrid materials holding wide perspectives for a broad range of applications, some of which have already been explored and are discussed in the following.

4.1. Spin Probes and Spin Labels

The paramagnetic radical species supported on Au NPs have been mainly used to report information of other systems or processes when they are used as added species (spin probes) to the studied system or when they are covalently bonded to the system (spin labels). Both spin probes and spin labels are commonly followed by ESR.[59]

TEMPO, TEMPONE, and TEMPAMINE were used as spin probes in the study of the interactions between these paramagnetic species and the Au NPs.[52] A loss of the ESR signal in the absence of oxygen was observed upon the adsorption of the radicals on the surface of the NPs. To prove the integrity of the radical molecule upon adsorption to the gold surface, the addition of ethanolamine to the TEMPAMINE-Au solutions resulted in the 95% recovery of the ESR signal and, thus, concluding that the loss of the signal intensity does not come from an irreversible reaction. Moreover, the use of small particles of 2.5 nm diameter allowed Au NPs containing an average of only 1.6 radicals per particle, therefore, ruling out the possible complete broadening of the ESR signal due to the dipole−dipole interaction between several radicals on the same particle. Additionally, since the surface-plasmon band of the Au NPs remained unchanged upon adsorption of the radicals, the electron density at the surface was essentially unchanged and, thus, a partial transfer of the unpaired electron to/from the particle was discarded as the cause of the observed loss of the signal. Further experiments showed that the diminishment of the averaging free tumbling of the radicals at the surface could not mask the signal produced by the nitroxyl radical. Considering all above data, the authors suggested that the reduction of the ESR signal occurs due to the exchange interaction of the unpaired electrons with conduction-band electrons of the metallic particle.

More recently, another specific application has arisen from the interest in studying membrane mimetic systems. This has driven the study of the exchange of different nitroxyls between the aqueous phase and the monolayers of different water−soluble protected gold clusters (Figure 12a).[53] The ESR spectra clearly showed two sets of signals due to the radical hosted in the AuNP monolayer and the free radical in solution, demonstrating the inclusion of the nitroxyl probes into the more hydrophobic environment of the monolayer (Figure 12a). The changes of the ESR spectrum are the alteration of the nitrogen hyperfine coupling, induced by the different polar environments in the presence of the host, and the strong reduction of the benzylic protons coupling, $a(2H_\beta)$, due to conformation changes occurring upon complexation. Moreover, it has been demonstrated that the observed signal modification resulting from the exchange process allows for the differentiation of the hydrophobicity of the monolayer, i.e. monolayers based on thiolates that differ by an alkyl or a perfluorinated chain.[54] Remarkably, these latter perfluorinated amphiphiles are characterized by a hydrophilic part that contrasts with the high hydrophobicity of the perfluorocarbon region; thus, they are soluble in polar solvents. The combination of the known biocompatibility of fluorinated compounds with these solubility properties makes these surfactants very interesting for applications in materials science and in the biomedical field, such as antioxidant carriers, or in the development of multicomponent nanoparticles with the capacity to store and release drug molecules. In this particular study, the interaction of a hydrophobic radical probe with the fluororinated part of the monolayer was investigated by performing ESR measurements.[54] Further investigation elucidated that the size of the metallic core gave different solvating properties to the protective organic monolayer, that is, different capacity to host an organic radical probe.[80]

The second main application of the paramagnetic species adsorbed on gold nanoparticles is the use as spin-labeled NPs. Several research groups have devoted their efforts to the understanding of the mechanistic aspects of ligand exchange in Au nanoparticles, since it is crucial for the rational design of nanoparticle-based nanocarriers and devices.[55a,h,81] The sensitivity of ESR spectroscopy to the interactions between adjacent paramagnetic species has been exploited to monitor the exchange of ligands between spin labeled and unlabeled AuNPs.[56] From the X-band ESR spectra of spin-labeled NPs in frozen solutions, a quantitative analysis of the dipole−dipole interactions between multiple spin labels adsorbed on the same Au nanoparticles can be performed with an indication of their distribution on the NP surface and the conformation of the adsorbed ligands.[82] In this way, the lateral diffusion of the thiolate ligands on the AuNPs was investigated by pulsed ESR. This was achieved by functionalizing the AuNPs with a ligand containing two spin labels connected by a cleavable ester bridge (Figure 12d).[55g] An evident spin−spin interaction was observed previous to the cleavage of the bridge, and only a slight increase of the distance between the two branches was observed after breaking the bridge. The results suggested that at room temperature the ligands possess virtually no lateral mobility but at elevated temperature (90 °C) some redistribution of the ligands on the surface takes place in several hours. Importantly, it was also demonstrated that the reactivity of Au nanoparticles in place-exchange with disulfides is greatly reduced by aging in solution at room temperature. The likely origin of this effect is a slow reorganization of the nanoparticle surface.[83]

Spin labeled AuNPs with pH-sensitive imidazoline nitroxyls have been used as a molecular probe technique for accessing interfacial surface electrostatics in the polar interface of water-soluble tiopronin-coated Au nanoclusters (Figure 12c).[55i]

These particles were labeled with the nitroxyls by ligand-exchange reaction, with an average labeling kept below one spin label per nanoparticle to avoid magnetic spin−spin interactions. The rate of proton exchange in the aqueous solution was observed in a change in the hyperfine coupling constant of the ESR spectrum. For example, the ESR spectra at intermediate pH were indicative of contributions from two species attributed to the protonated ($R^{\bullet}H^{+}$) and nonprotonated ($R^{\bullet}$) forms of the spin containing molecule. In view of this potential application of SAMs on gold to control the structure and function of biomolecules through tailoring interaction with the MPC surface and the pH sensitive nitroxyl lingands, it is expected to stimulate further research on the complex electrostatics of the organized monolayer interface and the phenomena of monolayer charge compensation upon DNA and/or protein binding.

Ruthstein et al. used 5DSA and 16DSA molecules (Figure 1) as spin labels to follow the adsorption process, the organization, and the exchange interactions between spins of the respective monolayers on a surface of GaAs with time.[46] The ESR spectra of 5DSA on GaAs recorded at $t = 0$ (just after removing from the adsorbents solution) and then following their evolution in time up to 24 h showed that the peaks corresponding to the ^{14}N hyperfine coupling became sharper, which was accounted for by a variation in the spin-exchange interaction between neighboring molecules due to a surface molecular reorganization. On the basis of the time evolution of the ESR line-shape, they concluded that initially the molecules are inhomogeneously distributed, exhibiting strong spin-exchange interactions, but with the time an annealing process takes place and the coverage becomes even, reducing the spin−spin interactions. The ESR spectra of a fresh and one week old 16DSA monolayer demonstrated that the organization of these SAMs is time independent and resembles those of the 5DSA at short time. The difference in behavior of 5DSA and 16DSA at longer times was attributed to higher coverage and denser packing of the 16DSA molecules on the surface, resulting in a closer interdistance and larger exchange interactions.

4.2. Porous Materials with Magnetic Properties

Metal−organic frameworks (MOFs) are hybrid inorganic−organic solid compounds with zeolite-like structures and properties. They show promise for an impressive number of applications in gas storage, drug-delivery, diagnostics, sensing, catalysis, ion exchange or separation, magnetism, optics, etc.[84b] One of the challenges in the field is the deposition or growth of MOFs on substrates for the preparation of devices which can exploit such interesting properties.[85] In this regard, SAMs with specific functionalization can serve as platforms for a controlled oriented growth of more complex structures, such as MOFs.[86] MOFs incorporating organic free radicals in their skeleton are part of the magnetic open frameworks family which could be used as magnetic data storage devices. For instance, $Cu_3(btc)_2$ (btc = 1,3,5-benzenetricarboxylate), also known as HKUST-1, is one of the most investigated MOF materials in the solid state. The modification of its magnetic properties by adsorption of suitable guest molecules is of particular interest. Recently, Jee et al. discussed the suppression of the antiferromagnetic coupling of the Cu(II) ions in the paddle-wheel building blocks of the metal−organic framework compound $Cu_3(btc)_2$ by interaction with the di-*tert*-butyl nitroxyl (DTBN) radicals and the subsequent formation of the $S = {}^1/_2$ copper centers.[87] Some of us prepared a series of MOFs using the polychlorinated triphenylmethyl tricarboxylic acid radical PTMTC as a polytopic ligand with an organic free radical nature.[88] The strategy used for such MOFs consisted in combining this radical ligand with magnetically active transition metal ions. These structures showed larger magnetic couplings and dimensionalities, since the radical acted as a magnetic relay. Successfully, purely organic magnetic open frameworks based on these carboxylic functionalized PTM radicals linked by H-bonds were also reported.[28,89]

With the final aim to grow on a surface this latter MOF example based on PTMTC radical and Cu(II) ions, as a first approximation the PTMCOOH radical was grafted to a SAM with suitable ending groups through cooper(II), following the layer-by-layer approach, as explained in section 2.2 (Figure 9d, SAM **S4** in Figure 10).[50d] However, this organic ligand only has one coupling unit, so for this reason only the deposition of one monolayer could be achieved. This layer-by-layer procedure is a promising route for the construction of extended porous and magnetic PTM-based coordination polymers confined on surfaces. The use of PTM radicals functionalized with various binding groups to grow multiple layers is currently under investigation.

4.3. Electrocatalysis

TEMPO and its derivatives, under their ammonium form, have been extensively studied as redox mediators for the oxidation of organic compounds in solution, especially for oxidizing primary alcohols.[75] For practical applications, the immobilization of such nitroxyl radicals on electrodes coated with a polymer film has been pursued for many years.[90] As an alternative, the preparation of modified electrodes with SAMs of these radicals for electrocatalysis was initiated by Fuchigami already in 1997.[91] They prepared a modified gold electrode with a self-assembled D,L-α-lipoic acid derivative bearing a TEMPO radical. They observed that to have stable electroactive SAMs it was necessary to coadsorb the radical on the surface with small amounts of unsubstituted alkanethiols. Such modified electrodes were successfully applied to carry out electrocatalytic oxidation of 4-methylbenzyl alcohol and α-phenethyl-amine in acetonitrile.

Later on, Kashiwagi et al. reported on the preparation of mixed SAMs based on a chiral TEMPO-terminated thiol and hexadecanethiol for enantioselective electrocatalysis.[92] The enantioselective oxidation of a chiral secondary alcohol was investigated using (*R*)-(+)- and (*S*)-(−)-1-phenylethanol. The CVs of these compounds in the presence of 2,6-lutidine (Figure 17a) show that the anodic peak current for (*S*)-(−)-1-phenylethanol was highly enhanced in comparison with the blank voltammogram, and no cathodic peak was observed on the reverse scan, demonstrating that the alcohol had been efficiently oxidized in an irreversible manner. On the contrary, the anodic peak current of the CV of (*R*)-(+)-1-phenylethanol only increased slightly. The authors stated that this modified electrode could be useful for the determination of the optical purity of a racemic mixture of a secondary alcohol. On the other hand, this electrode functionalized with the chiral-TEMPO did not exhibit enantioselectivity in the oxidation of primary alcohols such as (2-phenyl-1-propanol) (Figure 17b), indicating that the hydroxyl group of the alcohols had to be directly attached to the chiral carbon to be discriminated by the chiral-TEMPO SAM in the oxidation reaction. The same functionalized gold electrode was also applied for the enantioselective oxidation of chiral amines. The electrocatalytic oxidation of a series of amines was investigated in acetonitrile, and similarly to the case explained before, it was found that the enantioselective oxidation only occurred when an α-hydrogen of the chiral center was adjacent to the amino group.[93]

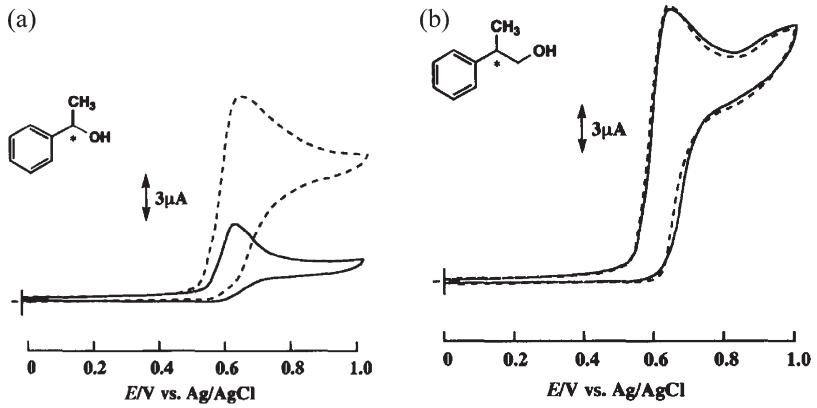

Figure 17. Cyclic voltammograms of a chiral-TEMPO modified gold electrode in 0.1 M $NaClO_4/CH_3CN$ at 100 mV/s in the presence of (a) 10 mM (*R*)-(+)-1-phenylethanol (continuous line) or (*S*)-(−)-1-phenylethanol (dashed line) and 20 mM 2,6-lutidine and (b) 10 mM (*R*)-(+)-2-phenyl-1-propanol (continuous line) or (*S*)-(−)-2-phenyl-1-propanol (dashed line) and 20 mM 2,6-lutidine. Reprinted with permission from ref 92. Copyright The Electrochemical Society of Japan 1999.

More recently, mixed and single component SAMs of TEMPO-SH 1−3 were shown to reveal electrocatalytic activities toward benzyl-alcohol oxidation in both aqueous and nonaqueous solvents.[43] It was observed that mixed SAMs of TEMPO-SH 1−3 with alkanethiols (up to a dilution limit) enhance the absolute catalytic current, in spite of having only few immobilized electroactive centers, and they improve the stability of the electrocatalitic process.

Finally, the anodization of glassy carbon electrodes permitted functionalization of them with oligo(ethylene glycol), which was then used to graft effectively 4-amino-TEMPO via the formation of an amide bond.[94] These electrodes also demonstrated good and stable electrocatalytic ability for the oxidation of allyl alcohol in the presence of 2,6-lutidine.

4.4. Electrical Transport and Spintronics

The field of molecular electronics has attracted a vast amount of research work over the last few decades due to its potential for technological applications combined with the intrinsic characteristics of organic materials such as lightweight, flexibility, processability, and tunable properties by chemical synthesis. However, most of the investigations have been mainly focused on the charge carrier transport through the organic systems, and only recently is effort being placed on exploring their spin transport properties (i.e., spin injection and spin conservation) due to the high potential in applications such as novel spin-based magnetic recording and memory devices. This novel field is known as molecular spin electronics or molecular spintronics.[95] Due to their weak spin−orbit coupling and hyperfine interactions, organic molecules are considered to be ideal media for spin transport, in which spin coherence over time and distance could be preserved much longer than in inorganic materials. The latter are used nowadays in conventional spintronic devices. The utilization of organic radicals as linkers between conducting contacts in spintronic devices could favor the spin polarization conservation during the transport process.[96]

In this direction, a pioneering work based on measuring the transport properties of a network of gold nanoparticles interconnected by spin polarized molecular wires (SPM) was carried out by Sugawara et al.[97] Such SPM systems consisted of a spin polarizing donor core based on a α-nitronyl nitroxyl radical, a conjugated thiophene-pyrrole-thiophene trimer, and disulfide groups to graft on Au (Figure 18a).[97d] As reference, a spinless wire molecule (SLM) was also tested grafted on AuNPs. Since the employed gold NPs had an average diameter of 4 nm, they exhibit a very low self-capacitance, and hence, the charging energy of a single NP is higher than the thermal energy. Therefore, at low temperature these NPs work as Coulomb islands. The dependence of the conductance of both SPM and SLM networks with NPs measured deposited on interdigidated electrodes revealed a thermal activation type behavior above 30 K. Below this temperature, it was suggested that inelastic cotunneling processes, in which electrons simultaneously tunnel through more than one junction without paying the cost of charging energy, were dominating. In addition, the conductance of the SPM network in the lower *T* range was inferior to that of the SLM network, indicating that the isolated spin on the wire molecules disrupted the cotunneling process (Figure 18b). This could be explained by considering that the electron that tunnels between two gold NPs connected through a SPM wire undergoes spin-flip scattering due to exchange interaction with the localized spin on the radical unit of the wire (Figure 18c). In such a case, two-tunneling processes across one NP can no longer be coherent. Interestingly, the conductance of the SPM network increased with an increasing external magnetic field applied perpendicular to the device, yielding a magnetoresistance of −2.5% at a field of 6 T (Figure 18b).[97d] On the other hand, only slightly positive magetoresistance was observed for the SLM network. The effect can be accounted for by the fact that the magnetic field promotes a preferable orientation of localized spins, suppressing then the spin-flip scattering and recovering the probability of cotunneling. This is the first experimental example reported in which it is shown that the organic localized spin of a radical interacts with itinerant conducting electrons, a fundamental step to develop spintronic devices.

A different approach focusing on exploring the transport properties of SAMs of organic radicals has been followed by us.[50c,98] The transport properties of SAMs based on the radical as well as on the closed-shell form of a PTM derivative (i.e., PTM(rad)-SAM and PTM(αH)-SAM, respectively) on gold were studied. These two systems give rise to SAMs with no significant structural molecular variations but with extremely different electronic structure that is responsible for the large difference in the conducting properties observed. This investigation proceeded on SAM **S2b** (Figure 10) and on its closed-shell form based SAM.[50c] To study comparatively the transport

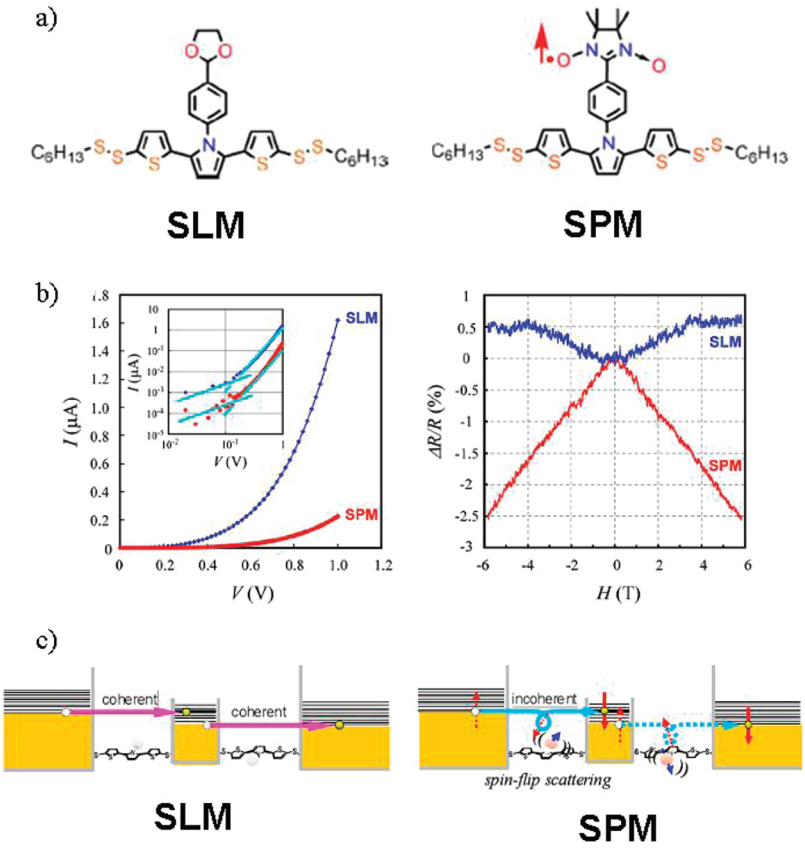

Figure 18. (a) Molecular structure of the SPM and SLM wires. (b) Left. Current−voltage characteristics in SLM and SPM networks (T = 4.2 K). The inset displays log−log plots. Right. Magnetoresistance of SPM and SLM networks at 4.2 K (1 V). (c) Left. Cotunneling across the nanoparticle of the SLM network. Right. Spin-flip scattering of tunnel electrons by a local spin in the SPM network. Reprinted with permission from ref 97d. Copyright The American Physical Society 2008.

characteristics of both SAMs, the 3D operation mode of conducting scanning force microscopy (C-SFM) was employed, which allows the simultaneous measurement of the normal force (F_n) and the current (I) as a function of the bias voltage (V) and controlling the sample displacement distance toward the tip (z).

The $I(V,z)$ images acquired on the PTM(αH)-SAM (left) and the PTM(rad)-SAM (right) PTM are depicted in Figure 19a and confirm that both SAMs exhibit different transport behaviors. Horizontal profiles taken in the image are the $I-V$ curves corresponding to each piezo displacement value. After the jump into the contact point, the central region (intermediate color) of the $I(V,z)$ image for PTM(rad)-SAM narrows, leading to a triangular shape typical of a monotonic pseudogap reduction, whereas for PTM(αH)-SAM the image shows a region with a fairly constant width. This striking difference occurs in a wide range of tip−sample distances, indicating that it is intrinsically due to the distinct electronic characteristics of the two PTM-SAMs. The observed behavior can be more clearly observed and even quantified in the selected representative $I-V$ profiles (marked with three different symbols ■, ●, ▲) taken at different applied loads (Figure 19b). When just entering in contact (■), no current is measured in either SAM. At 5 nN of applied load (●), the tip−SAM−gold junction is formed, since current is measured in both monolayers. Both $I-V$ curves exhibit a sigmoidal shape over the ±2 V voltage range with a linear response in the low bias region steeper for the radical PTM monolayer. By increasing the applied load up to 15 nN (▲), this difference becomes more evident, indicating that the conductivity through the PTM(rad) SAM is much higher than that through the PTM(αH) SAM. Remarkably, it was found that the PTM(rad) SAM shows a junction resistance (10−40 MΩ) 1 order of magnitude smaller than that of the PTM(αH) SAM (200−300 MΩ).

Density functional calculations were employed to gain further insight into the electronic structures of each molecule and to understand the transport mechanisms (Figure 19c). The PTM(αH) has a large energy HOMO−LUMO gap (~5 eV), while the PTM(rad) has a SOMO in the α spin with a similar energy to the PTM(αH) HOMO but a significantly lower energy LUMO in the β spin compared to the LUMO of the PTM(αH). This LUMO-β of PTM(rad) has an energy significantly closer to the Fermi levels of both Au- and B-doped CVD diamond (used as a tip) than the LUMO in PTM(αH). It was suggested thus that in the case of the PTM(αH) SAM, since the Fermi level of the contacts employed lies in the large HOMO−LUMO gap, the transport probably follows a nonresonant tunneling mechanism. However, since the LUMO-β level of PTM(rad) approaches the metal Fermi levels, LUMO-assisted transport could take place and some contribution of resonant tunneling could be expected. Finally, it is also possible to speculate that the large energy difference between the SOMO and the LUMO-β of the PTM(rad) SAM opened the interesting possibility of whether this system could give rise to spin polarized transport by acting as a spin filter.

Very recently, we have also investigated the closed and open-shell forms of a fully conjugated PTM derivative hybridized with a

dx.doi.org/10.1021/cr200233g |*Chem. Rev.* 2012, 112, 2506–2527

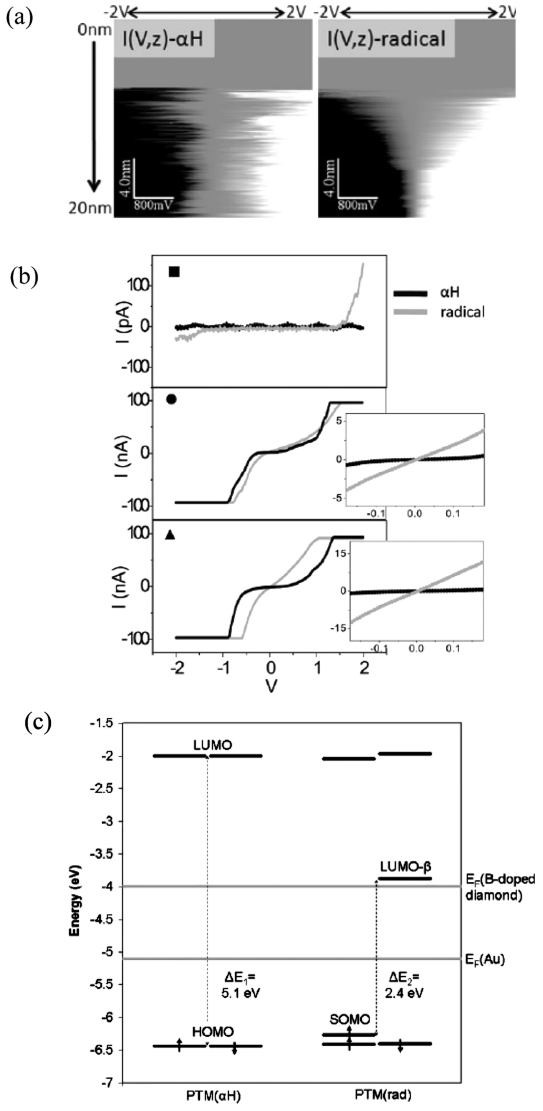

Figure 19. (a) Current image, $I(V,z)$, acquired on the αH (left) and radical (right) PTM-SAMs. (b) Selected horizontal line profiles extracted from the images in part a at different applied loads. Insets: linear region of the $I-V$ curve ($\pm$0.2 V). (c) Energy levels obtained from DFT calculations for PTM (αH) and PTM (rad) derivatives. Reprinted with permission from ref 50c. Copyright 2009 Wiley-VCH Verlag GmbH and Co.

gold substrate (**S1a**, Figure 10).[98] Similar transport characteristics were observed here, since the resistance of the radical SAM was 2 orders of magnitude lower than that of the nonradical one. Additionally, it was found that both SAMs (i.e., the open and closed-shell forms) revealed negative differential resistances (NDR) in their $I-V$ curves at high voltage, which were attributed to similar resonant tunneling with unoccupied molecular orbitals.

The exciting field of molecular spintronics has also attracted theoretical scientists to explore the spin transport properties through organic radicals, and a series of reports have already appeared predicting the potential of these paramagnetic species as spin filters.[99] However, it should be mentioned that in all these analyses spin flips were neglected. For example, the calculated coherent transport properties of polyphenoxyl radical with four radicals centers sandwiched between two electrodes showed that the majority (α) and minority (β) spin components exhibit considerably different transmission spectra in the vicinity of the Fermi level. Therefore, if the magnetization axis is fixed by an external magnetic field, the molecular bridge would work as a spin filter.[99b]

More recently, the transport properties of benzene-based model radicals were also predicted to differ to a sufficient extent for electrons of different spins.[99c] Also, these radicals could be tuned systematically by introducing substituents, giving them a more preferential transport for either the α or β spin component. These predictions could also be transferred to some larger stable radicals with which experimental tests could be done

Along this line, the transport properties of a family of 1,4-benzenediamines bridging two Au electrodes were also modeled.[99a] The molecules were substituted in the 2-position with the radicals $-CH_2^{\bullet}$, $-NH^{\bullet}$, and $-O^{\bullet}$. The spin filter efficiencies for these systems were calculated to be 49%, 27%, and 1%, respectively. The differences were attributed to the different electron affinities of the radicals, since they found that the radicals once connected to the electrodes can accept some charge, reducing the excess of spin, which, in turn, reduces the molecular orbitals splitting and the spin filter efficiency.

Undoubtedly, the emerging *molecular spintronics* field is bound to progress dramatically in the next few years and certainly will bring new fundamental insights as well as fresh perspectives for the molecular devices of the future.

4.5. Molecular Switches and Memories

The functionalization of surfaces with molecules that can store data is of great importance for the development of today's information technology, since it would permit fabrication of ultrahigh density devices, down to the molecular level, which would also exhibit other interesting characteristics, such as flexibility and lightweight. As a consequence, bistable systems that undergo chemical or physical changes upon optical, magnetic, or electric external stimulation are required. The use of electroactive organic free radicals as molecular switches offers new opportunities in this field, since they allow electrochemically triggering not only the optical but also the magnetic response. In particular, PTM radicals are promising building blocks for this purpose, since they are electrically commutable in a reversible way between two easily accessible, stable, and persistent redox states (i.e., PTM radical and PTM anion), which reveal distinct magnetic and optical properties that can be employed as read-out mechanisms. Indeed, as mentioned before, PTM radical is a paramagnetic species with a maximum absorbance centered at 385 nm and a fluorescence emission in the red region of the spectrum, while the anion is diamagnetic with a maximum absorbance at around 510 nm and does not emit fluorescence.

The optical properties of PTM SAMs on quartz (surface **S2a**, Figure 10) revealed the characteristic absorption band of PTM radical moieties.[50a] After reduction of this SAM with tetrabutylammonium hydroxide, the radical absorption band completely disappeared and, instead, an absorption band coming from the PTM anion species was observed. This work elucidated that these multifunctional radical SAMs behave as chemical switches.

Lately, a highly robust surface confined switch based on a PTM radical on ITO (surface **S1c**, Figure 10) has been reported (Figure 20a).[50e] The electrochemical characteristics of these PTM radical SAMs were investigated by CV. As expected, one reversible redox wave was observed with an oxidation peak at +53 mV and a reduction peak at -32 mV at the scan rate 100 mV/s. The optical absorption, optical emission, and magnetic responses were employed to read the state of this multichannel switch.

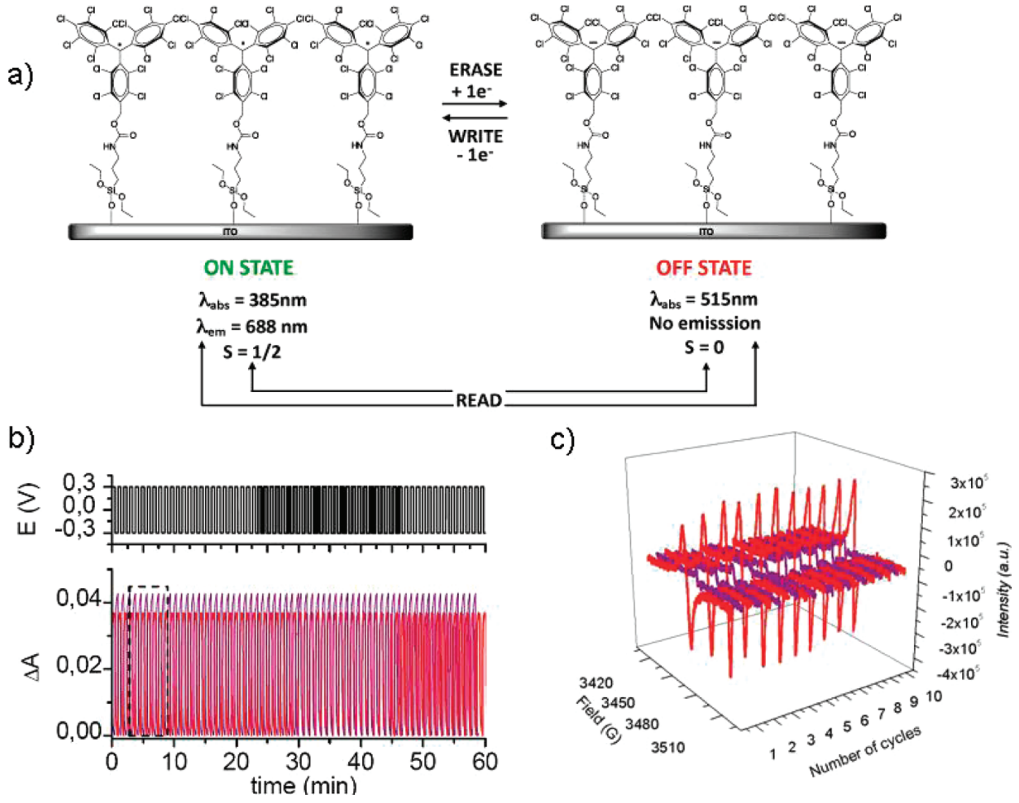

Figure 20. (a) Representation of the electrochemical bistability of a surface **S1c**. (b) Register of the optical response of **S1c**. Bottom: Optical response along time during sixty-five consecutive write-erase cycles (+0.3 V/−0.3 V vs Ag (s)) applied to the surface monitored at 385 nm (red line) and 515 nm (purple line). The electrochemical experiment was performed in situ using a UV−vis cuvette, an Ag wire as reference electrode, and an electrolyte solution of 0.02 M tetrabutylammonium hexafluorophosphate in acetonitrile. Top: Voltage profile applied to **S1c**. (c) Register of the magnetic response of **S1c**. EPR signal of the SAM **S1c** in air upon application of ten ON/OFF switching cycles. Red corresponds to the ON state (radical) and purple the OFF state (PTM anion). Reprinted with permission from ref 50e. Copyright Nature 2011 Publishing Group.

In the three cases, the reversibility of the switch was explored while performing write-erase cycles, switching **S1c** between the radical (ON state) and the anion (OFF state) form. The absorption bands characteristic from the two redox states changed simultaneously in opposite directions, following the profile of the applied voltages, in a completely reversible way and recovering completely the absorption intensity after each cycle (Figure 20b). Also, the fluorescence emission was switched off/switched on when reduction and oxidation cycles were applied. In turn, ESR experiments demonstrated that the ESR signal, corresponding to the PTM radical immobilized on the surface, disappeared upon reduction to the anionic form and appeared again after further oxidation, corroborating that the magnetic output was also a suitable read-out tool to determine the state of the switch (Figure 20c). The potential of this system to build nonvolatile memory devices was also demonstrated when a sequence of write−read−erase−read pulses were applied. Noteworthy is the fact that even after three months at ambient conditions the switch continued to be operating reliably, which is clear evidence that surface confined organic radicals can exhibit an outstanding stability. Further, the functional PTM molecules have been locally confined on a micrometer-sized spot on the ITO substrate employing the microcontact printing technique and using a microelectrode to apply the input stimules. Such a configuration enabled us to demonstrate the local addressability of the molecular switch. A point worth mentioning is that there is no foreseeable limitation to apply such a molecular switch to isolated molecules on a surface leading to molecule-scale memory devices. The reported system constitutes therefore a very promising platform for developing nonvolatile molecule-based memory devices based on immobilized free radicals.

More recently, the same optical and magnetic switching properties upon the application of an electrical external stimulus were found on the PTM functionalized Au surface **S1b**, when a very thin layer of gold was used.[50f] In addition, it was also shown here that the switch could also be read following the surface wettability. Taking into account the high hydrophobicity of PTMs due to the chlorine groups and that the reduced form of this SAM is an ionic species, the change of the surface wetting properties in the switching process was followed by monitoring the water contact angle. The SAM of the PTM radical changed from an average contact angle value of 102 ± 6° to 73 ± 3° for the PTM anion SAM. This reversible difference (∼29°) in the contact angle is rather high for a self-assembled monolayer. Such systems, able to tune their wetting properties reversibly, are currently raising an increased interest for the development of self-cleaning surfaces, microfluidics, and (bio)sensors.[3a,4b,100]

5. SUMMARY

Organic/inorganic hybrid materials based on attaching functional molecules to a surface are attracting great attention due to the wide range of novel properties and applications that these new materials can bring. Additionally, the use of organic molecules for surface functionalization opens the possibility to tune

the material properties and molecular assembly through synthetic chemistry. A particularly appealing field is focused on employing as an active molecular unit an organic free radical to anchor on a substrate either chemically or by physisorption. However, and unavoidably, the first question that arises when an organic free radical is deposited/grafted on a surface is what is the implication of their organization and relative arrangement of the neighboring radicals as well as their orientation with respect to the surface on their properties. Thus, a crucial issue is whether in these surface radical organizations, especially when conducting surfaces are employed, the magnetic properties of the molecules are preserved. This has prompted the application to these systems of several magnetic characterization techniques as well as theoretical studies, and in most of the cases, it has been found that the spin of the molecule is maintained after surface grafting. To further progress in this area, it is imperative to not only synthesize promising functional molecules able to form stable and robust surface assemblies but also to develop sensitive characterization techniques to read, or even modify (i.e., write), the surface properties. In most of the reported cases in which the radicals were covalently attached to a surface, hybrid materials exhibiting high robustness were achieved, offering wide perspectives for these materials. Hence, some of the traditional applications of organic free radicals have already been transferred to SAMs of these molecules on surfaces, such as spin-probe and spin-label functions, preparation of magnetic materials, and as catalysts in oxidation processes of organic molecules. In addition, an emerging and potential application that is growing large expectations is their use for the fabrication of *spintronic devices*, where the unpaired electron of the free radical could favor spin polarization conservation during the electron transport process. Further, the magnetic properties of bistable radicals have also been successfully exploited as an output signal in surface-confined molecular switches that could in the future lead to single molecule switching devices. In all likelihood, these novel hybrid materials based on attaching organic free radicals on surfaces will continue to arouse the interest of materials scientists in the coming years, since a wide range of interdisciplinary applications are foreseen.

AUTHOR INFORMATION

Corresponding Author

*E-mail: mmas@icmab.es; vecianaj@icmab.es.

BIOGRAPHIES

Marta Mas-Torrent received her Ph.D. in 2002, working at the Institut de Ciència de Materials, Consejo Superior de Investigacions Científicas (ICMAB-CSIC), in Barcelona, Spain, and at The Royal Institution of Great Britain in London, U.K. Afterward, she carried out postdoctoral research at the Kavli Institute of Nanoscience, Delft, The Netherlands. In November 2004 she came back to ICMAB with a Ramón y Cajal fellowship, and in June 2007 she obtained a tenured research position at ICMAB-CSIC. Her scientific interests include molecular electronics, organic field-effect transistors, multifunctional molecular materials, molecular switches and memory devices, self-assembly, and surface molecular organizations.

Núria Crivillers received her university degree in Chemistry from the Universitat Autònoma de Barcelona. She finished her Ph.D in 2008 at the Institut de Ciència de Materials (ICMAB-CSIC) in Barcelona, Spain. Her research activity continued with a postdoctoral stage in the group of Prof. Paolo Samorì at the Institut de Science et d'Ingénierie Supramoléculaires (UdS-CNRS) in Strasbourg (France), where she focused her research on the development of optically tunable field-effect transistors. She had recently joined the ICMAB-CSIC under the JAE program. Her research activities include self-assembled electroactive materials on surfaces and molecular data storage devices.

Concepció Rovira received her Ph.D. in Chemistry from the University of Barcelona. She trained as a postdoctoral fellow at CSIC in Barcelona and at Johns Hopkins University, MD, with Prof. D. O. Cowan. In 1987 she joined CSIC-CID with a Tenured Research position and became Full Professor at ICMAB-CSIC in 2004. Her research interests focus on multifunctional

molecular materials and molecular nanoscience and, in particular, on the fields of organic conductors, crystal engineering, supramolecular and surface self-assembling, electron-transfer processes, and molecular magnetism.

Jaume Veciana (Institut de Ciencia de Materials de Barcelona, ICMAB-CSIC) was appointed as Colaborador Cientifico of the CSIC in 1979 and in 1982/1983 moved to The Johns Hopkins University, MD (USA), as a postdoctoral fellow working on molecular conductors and organic metals. In 1991 he moved to the ICMAB, where was promoted to Full Professor in 1996. He coauthored more than 370 journal articles and book chapters and 15 patents, and edited two books, receiving in 2001 the Solvay Award and in 2004 the Real Sociedad de Quimica Española Award for his research in chemistry. In 2005 he received the DuPont Award for his contributions in Molecular Nanoscience and Nanotechnology. His research interests focus on molecular functional materials and molecular nanoscience.

ACKNOWLEDGMENT

We thank the EU Large Project One-P (FP7-NMP-2007-212311), the Networking Research Center on Bioengineering, Biomaterials and Nanomedicine (CIBER-BBN), the DGI (Spain), with projects CTQ2006-06333/BQU and CTQ2010-195011/BQU, and Generalitat de Catalunya (Grant 2009SGR00516).

REFERENCES

(1) Love, J. C.; Estroff, L. A.; Kriebel, J. K.; Nuzzo, R. G.; Whitesides, G. M. *Chem. Rev.* **2005**, *105*, 1103.

(2) (a) Basabe-Desmonts, L.; Beld, J.; Zimmerman, R. S.; Hernando, J.; Mela, P.; García Parajó, M. F.; van Hulst, N. F.; van den Berg, A.; Reinhoudt, D. N.; Crego-Calama, M. *J. Am. Chem. Soc.* **2004**, *126*, 7293. (b) de Ruiter, G.; Gupta, T.; van der Boom, M. E. *J. Am. Chem. Soc.* **2008**, *130*, 2744. (c) Diez-Gil, C.; Martinez, R.; Ratera, I.; Hirsh, T.; Espinosa, A.; Tarraga, A.; Molina, P.; Wolfbeis, O. S.; Veciana, J. *Chem. Commun.* **2011**, *47*, 1842.

(3) (a) Artzy-Schnirman, A.; Brod, E.; Epel, M.; Dines, M.; Hammer, T.; Benhar, I.; Reiter, Y.; Sivan, U. *Nano Lett.* **2008**, *8*, 3398. (b) Mendes, P. M. *Chem. Soc. Rev.* **2008**, *37*, 2512.

(4) (a) Chaudhury, M. K.; Whitesides, G. M. *Science* **1992**, *256*, 1539. (b) Liu, Y.; Mu, L.; Liu, B.; Kong, J. *Chem.—Eur. J.* **2005**, *11*, 2622.

(5) Heimel, G.; Romaner, L.; Zojer, E.; Bredas, J.-L. *Acc. Chem. Res.* **2008**, *41*, 721.

(6) (a) van der Boom, M. E.; Evmenenko, G.; Yu, C.; Dutta, P.; Marks, T. J. *Langmuir* **2003**, *19*, 10531. (b) Yitzchaik, S.; Marks, T. J. *Acc. Chem. Res.* **1996**, *29*, 197.

(7) (a) Train, C.; Norel, L.; Baumgarten, M. *Coord. Chem. Rev.* **2009**, *253*, 2342. (b) *Stable Radicals. Fundamentals and Applied Aspects of Odd-Electron Compounds*; Hicks, R. G., Ed.; John Wiley & Sons: Chichester, 2010; p 606.

(8) Gatteschi, D.; Cornia, A.; Mannini, M.; Sessoli, R. *Inorg. Chem.* **2009**, *48*, 3408.

(9) Hicks, R. G. *Org. Biomol. Chem.* **2007**, *5*, 1321.

(10) (a) Morita, Y.; Nishida, S.; Murata, T.; Moriguchi, M.; Ueda, A.; Satoh, M.; Arifuku, K.; Sato, K.; Takui, T. *Nat. Mater.* **2011**, DOI: 10.1038/NMAT3142. (b) Nishide, H.; Oyaizu, K. *Science* **2008**, *319*, 737. (c) Nishide, H.; Suga, T. *Electrochem. Soc. Interface* **2005**, *14*, 32. (d) Suga, T.; Konishi, H.; Nishide, H. *Chem. Commun.* **2007**, 1730.

(11) Gabellieri, C.; Mugnaini, V.; Paniagua, J. C.; Roques, N.; Oliveros, M.; Feliz, M.; Veciana, J.; Pons, M. *Angew. Chem., Int. Ed.* **2010**, *49*, 3360.

(12) Matsuki, Y.; Maly, T.; Ouari, O.; Karoui, H.; Moigne, F. L.; Rizzato, E.; Lyubenova, S.; Herzfeld, J.; Prisner, T.; Tordo, P.; Griffin, R. G. *Angew. Chem., Int. Ed.* **2009**, *48*, 4996.

(13) Caro, J.; Fraxedas, J.; Jürgens, O.; Santiso, J.; Rovira, C.; Veciana, J.; Figueras, A. *Adv. Mater.* **1998**, *10*, 608.

(14) (a) Bai, C. L.; Zhang, P. C.; Zhu, D. B.; Han, M. Y.; Xu, Y.; Zhang, D. Q.; Liu, Y. Q. *J. Phys. Chem.* **1995**, *99*, 8202. (b) Xu, Y.; Zhang, D. Q.; Zhang, P. C.; Liu, Y. Q.; Han, M. Y.; Zhu, D. B. *Thin Solid Films* **1996**, *284*, 537. (c) Zhang, D. Q.; Xu, Y.; Ding, L.; Liu, Y. Q.; Zhu, D. B. *Chem. Phys. Lett.* **1999**, *304*, 236.

(15) Hyakutake, T.; Park, J. Y.; Yonekuta, Y.; Oyaizu, K.; Nishide, H.; Advincula, R. *J. Mater. Chem.* **2010**, *20*, 9616–9618.

(16) (a) Hemme, W. L.; Fujita, W.; Awaga, K.; Eckert, H. *Dalton Trans.* **2009**, 7995. (b) Hemme, W. L.; Fujita, W.; Awaga, K.; Eckert, H. *J. Solid State Chem.* **2009**, *182*, 3330.

(17) (a) Karimi, B.; Biglari, A.; Clark, J. H.; Budarin, V. *Angew. Chem., Int. Ed.* **2007**, *46*, 7210. (b) Oliveros, M.; González-García, L.; Mugnaini, V.; Yubero, F.; Roques, N.; Veciana, J.; González-Elipe, A. R.; Rovira, C. *Langmuir* **2011**, *27*, 5098.

(18) Schulte, B.; Tsotsalas, M.; Becker, M.; Studer, A.; De Cola, L. *Angew. Chem., Int. Ed.* **2010**, *49*, 6881.

(19) Gallani, J. L.; Le Moigne, J.; Oswald, L.; Bernard, M.; Turek, P. *Langmuir* **2001**, *17*, 1104.

(20) Pong, W.-T.; Durkan, C.; Li, H.; Harneit, W. *J. Scanning Probe Microsc.* **2006**, *1*, 55.

(21) (a) Kumar, A.; Whitesides, G. M. *Appl. Phys. Lett.* **1993**, *63*, 2002. (b) Xia, Y.; Rogers, J. A.; Paul, K. E.; Whitesides, G. M. *Chem. Rev.* **1999**, *99*, 1823.

(22) Bartlett, P. D.; Funahashi, T. *J. Am. Chem. Soc.* **1962**, *84*, 2596.

(23) Niermann, N.; Degefa, T. H.; Walder, L.; Zielke, V.; Steinhoff, H.-J.; Onsgaard, J.; Speller, S. *Phys. Rev. B* **2006**, *74*, 235424.

(24) Krukowski, P.; Klusek, Z.; Olejniczak, W.; Klepaczko, R.; Puchalski, M.; Dabrowski, P.; Kowalczyk, P. J.; Gwozdzinski, K. *Appl. Surf. Sci.* **2009**, *255*, 8769.

(25) Mugnaini, V.; Fabrizioli, M.; Ratera, I.; Mannini, M.; Caneschi, A.; Gatteschi, D.; Manassen, Y.; Veciana, J. *Solid State Sci.* **2009**, *11*, 956.

(26) Messina, P.; et al. *Meas. Sci. Technol.* **2008**, *19*, 115802.

(27) Grillo, F.; Mugnaini, V.; Oliveros, M.; Francis, S. M.; Choi, D.-J.; Rastei, M. V.; Limot, L.; Cepek, C.; Pedio, M.; Bromley, S. T.; Richardson, N. V.; Bucher, J.-P.; Veciana, J. *Submitted.*

(28) Maspoch, D.; Domingo, N.; Ruiz-Molina, D.; Wurst, K.; Vaughan, G.; Tejada, J.; Rovira, C.; Veciana, J. *Angew. Chem., Int. Ed.* **2004**, *43*, 1828.

(29) Crivillers, N.; Furukawa, S.; Minoia, A.; Heyen, A. V.; Mas-Torrent, M.; Sporer, C.; Linares, M.; Volodin, A.; Van Haesendonck, C.; Van der Auweraer, M.; Lazzaroni, R.; De Feyter, S.; Veciana, J.; Rovira, C. *J. Am. Chem. Soc.* **2009**, *131*, 6246.

(30) Nakanishi, T.; Miyashita, N.; Michinobu, T.; Wakayama, Y.; Tsuruoka, T.; Ariga, K.; Kurth, D. G. *J. Am. Chem. Soc.* **2006**, *128*, 6328.

(31) De Feyter, S.; De Schryver, F. C. *Chem. Soc. Rev.* **2003**, *32*, 139.

(32) Ribas, X.; Maspoch, D.; Wurst, K.; Veciana, J.; Rovira, C. *Inorg. Chem.* **2006**, *45*, 5383.

(33) Rovira, C. *Chem.—Eur. J.* **2000**, *6*, 1723.
(34) Pai, W. W.; Zhang, Z.; Zhang, J.; Wendelken, J. F. *Surf. Sci.* **1997**, *393*, L106.
(35) (a) Greene, M. E.; Guisinger, N. P.; Basu, R.; Baluch, A. S.; Hersam, M. C. *Surf. Sci.* **2004**, *559*, 16. (b) Guisinger, N. P.; Elder, S. P.; Yoder, N. L.; Hersam, M. C. *Nanotechnology* **2007**, *18*, 044011.
(36) Pitters, J. L.; Piva, P. G.; Tong, X.; Wolkow, R. A. *Nano Lett.* **2003**, *3*, 1431.
(37) Pitters, J. L.; Wolkow, R. A. *J. Am. Chem. Soc.* **2005**, *127*, 48.
(38) Hallback, A. S.; Poelsema, B.; Zandvliet, H. J. W. *Appl. Surf. Sci.* **2007**, *253*, 4066.
(39) Guisinger, N. P.; Greene, M. E.; Basu, R.; Baluch, A. S.; Hersam, M. C. *Nano Lett.* **2004**, *4*, 55.
(40) Piva, P. G.; DiLabio, G. A.; Pitters, J. L.; Zikovsky, J.; Rezeq, M.; Dogel, S.; Hofer, W. A.; Wolkow, R. A. *Nature* **2005**, *435*, 658.
(41) Robin, A.; Marnell, L.; Bjork, J.; Dyer, M. S.; Bermudez, P. S.; Haq, S.; Barrett, S. D.; Persson, M.; Minoia, A.; Lazzaroni, R.; Raval, R. *J. Phys. Chem. C* **2009**, *113*, 13223.
(42) Nuzzo, R. G.; Allara, D. L. *J. Am. Chem. Soc.* **1983**, *105*, 4481.
(43) Alévêque, O.; Seladji, F.; Gautier, C.; Dias, M.; Breton, T.; Levillain, E. *ChemPhysChem* **2009**, *10*, 2401.
(44) Finklea, H. O.; Madhiri, N. *J. Electroanal. Chem.* **2008**, *621*, 129.
(45) Krukowski, P.; Kowalczyk, P. J.; Krzyczmonik, P.; Olejniczak, W.; Klusek, Z.; Puchalski, M.; Gwozdzinski, K. *Appl. Surf. Sci.* **2009**, *255*, 3946.
(46) Ruthstein, S.; Artzi, R.; Goldfarb, D.; Naaman, R. *Phys. Chem. Chem. Phys.* **2005**, *7*, 524.
(47) Matsushita, M. M.; Ozaki, N.; Sugawara, T.; Nakamura, F.; Hara, M. *Chem. Lett.* **2002**, *31*, 596.
(48) Mannini, M.; Sorace, L.; Gorini, L.; Piras, F. M.; Caneschi, A.; Magnani, A.; Menichetti, S.; Gatteschi, D. *Langmuir* **2007**, *23*, 2389.
(49) Mannini, M.; Rovai, D.; Sorace, L.; Perl, A.; Ravoo, B. J.; Reinhoudt, D. N.; Caneschi, A. *Inorg. Chim. Acta* **2008**, *361*, 3525.
(50) (a) Crivillers, N.; Mas-Torrent, M.; Perruchas, S.; Roques, N.; Vidal-Gancedo, J.; Veciana, J.; Rovira, C.; Basabe-Desmonts, L.; Ravoo, B. J.; Crego-Calama, M.; Reinhoudt, D. N. *Angew. Chem., Int. Ed.* **2007**, *46*, 2215. (b) Crivillers, N.; Mas-Torrent, M.; Vidal-Gancedo, J.; Veciana, J.; Rovira, C. *J. Am. Chem. Soc.* **2008**, *130*, 5499. (c) Crivillers, N.; Munuera, C.; Mas-Torrent, M.; Simao, C.; Bromley, S. T.; Ocal, C.; Rovira, C.; Veciana, J. *Adv. Mater.* **2009**, *21*, 1177. (d) Shekhah, O.; Roques, N.; Mugnaini, V.; Munuera, C.; Ocal, C.; Veciana, J.; Woll, C. *Langmuir* **2008**, *24*, 6640. (e) Simão, C.; Mas-Torrent, M.; Crivillers, N.; Lloveras, V.; Artés, J. M.; Gorostiza, P.; Veciana, J.; Rovira, C. *Nat. Chem.* **2011**, *3*, 359. (f) Simão, C.; Mas-Torrent, M.; Veciana, J.; Rovira, C. *Nano Lett.* **2011**, *11*, 4382.
(51) Shekhah, O.; Wang, H.; Strunskus, T.; Cyganik, P.; Zacher, D.; Fischer, R.; Wöll, C. *Langmuir* **2007**, *23*, 7440.
(52) Zhang, Z. Y.; Berg, A.; Levanon, H.; Fessenden, R. W.; Meisel, D. *J. Am. Chem. Soc.* **2003**, *125*, 7959.
(53) Lucarini, M.; Franchi, P.; Pedulli, G. F.; Pengo, P.; Scrimin, P.; Pasquato, L. *J. Am. Chem. Soc.* **2004**, *126*, 9326.
(54) Gentilini, C.; Evangelista, F.; Rudolf, P.; Franchi, P.; Lucarini, M.; Pasquato, L. *J. Am. Chem. Soc.* **2008**, *130*, 15678.
(55) (a) Caragheorgheopol, A.; Chechik, V. *Phys. Chem. Chem. Phys.* **2008**, *10*, 5029. (b) Chechik, V.; Wellsted, H. J.; Korte, A.; Gilbert, B. C.; Caldararu, H.; Ionita, P.; Caragheorgheopol, A. *Faraday Discuss.* **2004**, *125*, 279. (c) Harada, G.; Sakurai, H.; Matsushita, M. M.; Izuoka, A.; Sugawara, T. *Chem. Lett.* **2002**, 1030. (d) Hata, K.; Fujihara, H. *Chem. Commun.* **2002**, 2714. (e) Ionita, P.; Caragheorgheopol, A.; Gilbert, B. C.; Chechik, V. *J. Am. Chem. Soc.* **2002**, *124*, 9048. (f) Ionita, P.; Gilbert, B. C.; Chechik, V. *Angew. Chem., Int. Ed.* **2005**, *44*, 3720. (g) Ionita, P.; Volkov, A.; Jeschke, G.; Chechik, V. *Anal. Chem.* **2008**, *80*, 95. (h) Ionita, P.; Wolowska, J.; Chechik, V.; Caragheorgheopol, A. *J. Phys. Chem. C* **2007**, *111*, 16717. (i) Khlestkin, V. K.; Polienko, J. F.; Voinov, M. A.; Smirnov, A. L.; Chechic, V. *Langmuir* **2008**, *24*, 609. (j) Templeton, A. C.; Hostetler, M. J.; Warmoth, E. K.; Chen, S. W.; Hartshorn, C. M.; Krishnamurthy, V. M.; Forbes, M. D. E.; Murray, R. W. *J. Am. Chem. Soc.* **1998**, *120*, 4845.
(56) Zachary, M.; Chechik, V. *Angew. Chem., Int. Ed.* **2007**, *46*, 3304.
(57) Krukowski, P.; Kozlowski, W.; Olejniczak, W.; Klusek, Z.; Puchalski, M.; Dabrowski, P.; Kowalczyk, P. J.; Gwozdzinski, K.; Grabowski, G. *Appl. Surf. Sci.* **2008**, *255*, 1921.
(58) Busolo, F.; Franco, L.; Armelao, L.; Maggini, M. *Langmuir* **2010**, *26*, 1889.
(59) Lucarini, M.; Pasquato, L. *Nanoscale* **2010**, *2*, 668.
(60) Durkan, C. *Contemp. Phys.* **2004**, *45*, 1.
(61) Wiesendanger, R.; Guntherodt, H.; Guntherodt, G.; Gambino, R. J.; Ruf, R. *Phys. Rev. Lett.* **1990**, *65*, 247.
(62) (a) Brede, J.; Atodiresei, N.; Kuck, S.; Lazic, P.; Caciuc, V.; Morikawa, Y.; Hoffmann, G.; Blugel, S.; Wiesendanger, R. *Phys. Rev. Lett.* **2010**, *105*, 047204. (b) Iacovita, C.; Rastei, M. V.; Heinrich, B. W.; Brumme, T.; Kortus, J.; Limot, L.; Bucher, J. P. *Phys. Rev. Lett.* **2008**, *101*, 116602.
(63) Manassen, Y.; Hamers, R. J.; Demuth, J. E.; Castellano, A. J., Jr. *Phys. Rev. Lett.* **1989**, *62*, 2531.
(64) Mannini, M.; Messina, P.; Sorace, L.; Gorini, L.; Fabrizioli, M.; Caneschi, A.; Manassen, Y.; Sigalotti, P.; Pittana, P.; Gatteschi, D. *Inorg. Chim. Acta* **2007**, *360*, 3837.
(65) (a) Durkan, C.; Welland, M. E. *Appl. Phys. Lett.* **2002**, *80*, 458. (b) Messina, P.; Mannini, M.; Caneschi, A.; Gatteschi, D.; Sorace, L.; Sigalotti, P.; Sandrin, C.; Prato, S.; Pittana, P.; Manassen, Y. *J. Appl. Phys.* **2007**, *101*, 053916.
(66) Gorini, L.; Fabrizioli, M.; Mannini, M.; Sorace, L.; Yakovenko, A. *Inorg. Chim. Acta* **2008**, *361*, 4089.
(67) Messina, P.; Fradin, F. *Langmuir* **2009**, *25*, 1885.
(68) Rogez, G.; Donnio, B.; Terazzi, E.; Gallani, J.-L.; Kappler, J.-P.; Bucher, J.-P.; Drillon, M. *Adv. Mater.* **2009**, *21*, 4323.
(69) (a) Gonidec, M.; Davies, E. S.; McMaster, J.; Amabilino, D. B.; Veciana, J. *J. Am. Chem. Soc.* **2010**, *132*, 1756. (b) Stepanow, S.; Mugarza, A.; Ceballos, G.; Moras, P.; Cezar, J. C.; Carbone, C.; Gambardella, P. *Phys. Rev. B* **2010**, *82*, 014405.
(70) Rugar, D.; Yannoni, C. S.; Sidles, J. A. *Nature* **1992**, *360*, 563.
(71) (a) Katoh, K.; Yoshida, Y.; Yamashita, M.; Miyasaka, H.; Breedlove, B. K.; Kajiwara, T.; Takaishi, S.; Ishikawa, N.; Isshiki, H.; Zhang, Y. F.; Komeda, T.; Yamagishi, M.; Takeya, J. *J. Am. Chem. Soc.* **2009**, *131*, 9967. (b) Komeda, T.; Isshiki, H.; Liu, J.; Zhang, Y. F.; Lorente, N.; Katoh, K.; Breedlove, B. K.; Yamashita, M. *Nat. Commun.* **2011**, *2*, DOI: 10.1038/ncomms.1210. (c) Zhao, A. D.; Li, Q. X.; Chen, L.; Xiang, H. J.; Wang, W. H.; Pan, S.; Wang, B.; Xiao, X. D.; Yang, J. L.; Hou, J. G.; Zhu, Q. S. *Science* **2005**, *309*, 1542. (d) Gao, L.; Ji, W.; Hu, Y. B.; Cheng, Z. H.; Deng, Z. T.; Liu, Q.; Jiang, N.; Lin, X.; Guo, W.; Du, S. X.; Hofer, W. A.; Xie, X. C.; Gao, H. J. *Phys. Rev. Lett.* **2007**, *99*, 106402.
(72) Salman, Z.; Chow, K. H.; Miller, R. I.; Morello, A.; Parolin, T. J.; Hossain, M. D.; Keeler, T. A.; Levy, C. D. P.; MacFarlane, W. A.; Morris, G. D.; Saadaoui, H.; Wang, D.; Sessoli, R.; Condorelli, G. G.; Kiefl, R. F. *Nano Lett.* **2007**, *7*, 1551.
(73) (a) Finklea, H. O.; Haddox, R. M. *Phys. Chem. Chem. Phys.* **2001**, *3*, 3431. (b) Sagara, T.; Midorikawa, T.; Shultz, D. A.; Zhao, Q. *Langmuir* **1998**, *14*, 3682.
(74) (a) Alévêque, O.; Blanchard, P.-Y.; Breton, T.; Dias, M.; Gautier, C.; Levillain, E.; Seladji, F. *Electrochem. Commun.* **2009**, *11*, 1776. (b) Alévêque, O.; Blanchard, P.-Y.; Gautier, C.; Dias, M.; Breton, T.; Levillain, E. *Electrochem. Commun.* **2010**, *12*, 1462. (c) Alévêque, O.; Gautier, C.; Dias, M.; Breton, T.; Levillain, E. *Phys. Chem. Chem. Phys.* **2010**, *12*, 12584. (d) Gautier, C.; Alévêque, O.; Seladji, F.; Dias, M.; Breton, T.; Levillain, E. *Electrochem. Commun.* **2010**, *12*, 79.
(75) (a) Sheldon, R. A.; Arends, I. W. C. E. *J. Mol. Catal., A: Chem.* **2006**, *251*, 200. (b) Sheldon, R. A.; Arends, I. W. C. E.; ten Brink, G.-J.; Dijksman, A. *Acc. Chem. Res.* **2002**, *35*, 774. (c) Bragd, P. L.; van Bekkum, H.; Besemer, A. C. *Top. Catal.* **2004**, *27*, 49.
(76) Bencini, A.; Rajaraman, G.; Totti, F.; Tusa, M. *Superlattices Microstruct.* **2009**, *46*, 4.
(77) Rajaraman, G.; Caneschi, A.; Gatteschi, D.; Totti, F. *J. Mater. Chem.* **2010**, *20*, 10747.
(78) Bennett, J. M.; Warschkow, O.; Marks, N. A. *J. Phys. Chem. C* **2009**, *113*, 1020.

(79) Mitsutaka, O.; Yasutaka, K.; Takeshi, T.; Kizashi, Y. *Polyhedron* **2005**, *24*, 2330.
(80) Lucarini, M.; Franchi, P.; Pedulli, G. F.; Gentilini, C.; Polizzi, S.; Pengo, P.; Scrimin, P.; Pasquato, L. *J. Am. Chem. Soc.* **2005**, *127*, 16384.
(81) Ionita, P.; Caragheorgheopol, A.; Gilbert, B. C.; Chechik, V. *Langmuir* **2004**, *20*, 11536.
(82) Ionita, P.; Caragheorgheopol, A.; Gilbert, B. C.; Chechik, V. *J. Phys. Chem. B* **2005**, *109*, 3734.
(83) Chechik, V. *J. Am. Chem. Soc.* **2004**, *126*, 7780.
(84) (a) Carne, A.; Carbonell, C.; Imaz, I.; Maspoch, D. *Chem. Soc. Rev.* **2011**, *40*, 291. (b) Special issue on metal−organic framework materials. *Chem. Soc. Rev.* 2009, *38*, 1201.
(85) Zacher, D.; Shekhah, O.; Woll, C.; Fischer, R. A. *Chem. Soc. Rev.* **2009**, *38*, 1418.
(86) (a) Altman, M.; Shukla, A. D.; Zubkov, T.; Evmenenko, G.; Dutta, P.; van der Boom, M. E. *J. Am. Chem. Soc.* **2006**, *128*, 7374. (b) Green, M. A. *Nat. Mater.* **2010**, *9*, 539. (c) Makiura, R.; Motoyama, S.; Umemura, Y.; Yamanaka, H.; Sakata, O.; Kitagawa, H. *Nat. Mater.* **2010**, *9*, 565. (d) Scherb, C.; Schodel, A.; Bein, T. *Angew. Chem., Int. Ed.* **2008**, *47*, 5777. (e) Walker, A. V. *Langmuir* **2010**, *26*, 13778. (f) Wanunu, M.; Vaskevich, A.; Shanzer, A.; Rubinstein, I. *J. Am. Chem. Soc.* **2006**, *128*, 8341.
(87) Jee, B.; Koch, K.; Moschkowitz, L.; Himsl, D.; Hartman, M.; Poppl, A. *J. Phys. Chem. Lett.* **2011**, *2*, 357.
(88) (a) Maspoch, D.; Ruiz-Molina, D.; Veciana, J. *Chem. Soc. Rev.* **2007**, *36*, 770. (b) Maspoch, D.; Ruiz-Molina, D.; Wurst, K.; Domingo, N.; Cavallini, M.; Biscarini, F.; Tejada, J.; Rovira, C.; Veciana, J. *Nat. Mater.* **2003**, *2*, 190.
(89) (a) Roques, N.; Maspoch, D.; Domingo, N.; Ruiz-Molina, D.; Wurst, K.; Tejada, J.; Rovira, C.; Veciana, J. *Chem. Commun.* **2005**, 4801. (b) Roques, N.; Maspoch, D.; Wurst, K.; Ruiz-Molina, D.; Rovira, C.; Veciana, J. *Chem.—Eur. J.* **2006**, *12*, 9238.
(90) (a) Yamauchi, Y.; Maeda, H.; Ohmori, H. *Chem. Pharm. Bull.* **1997**, *45*, 2024. (b) Kashiwagi, Y.; Ohsawa, A.; Osa, T.; Ma, Z.; Bobbitt, J. M. *Chem. Lett.* **1991**, 581. (c) Kashiwagi, Y.; Yanagisawa, Y.; Kurashima, F.; Anzai, J.; Osa, T.; Bobbitt, J. M. *Chem. Commun.* **1996**, 2745. (d) Osa, T.; Akiba, U.; Segawa, I.; Bobbitt, J. M. *Chem. Lett.* **1988**, 1423. (e) Osa, T.; Kashiwagi, Y.; Yanagisawa, Y.; Bobbitt, J. M. *J. Chem. Soc., Chem. Commun.* **1994**, 2535. (f) Yanagisawa, Y.; Kashiwagi, Y.; Kurashima, F.; Anzai, J.; Osa, T.; Bobbitt, J. M. *Chem. Lett.* **1996**, 1043. (g) Deronzier, A.; Limosin, D.; Moutet, J. C. *Electrochim. Acta* **1987**, *32*, 1643. (h) Merz, A.; Bachmann, H. *J. Am. Chem. Soc.* **1995**, *117*, 901.
(91) Fuchigami, T.; Shintani, T.; Konno, A.; Higashiya, S.; Nonaka, T. *Denki Kagaku* **1997**, *65*, 506.
(92) Kashiwagi, Y.; Uchiyama, K.; Kurashima, F.; Anzai, J.; Osa, T. *Electrochemistry* **1999**, *67*, 900.
(93) Kashiwagi, Y.; Uchiyama, K.; Kurashima, F.; Anzai, J.; Osa, T. *Anal. Sci.* **1999**, *15*, 907.
(94) Maeda, H.; Saka-iri, Y.; Ogasawara, T.; Huang, C. Z.; Yamauchi, Y.; Ohmori, H. *Chem. Pharm. Bull.* **2001**, *49*, 1349.
(95) Sanvito, S. *Chem. Soc. Rev.* **2011**, *40*, 3336.
(96) (a) Sugawara, T.; Matsushita, M. M. *J. Mater. Chem.* **2009**, *19*, 1738. (b) Mas-Torrent, M.; Crivillers, N.; Mugnaini, V.; Ratera, I.; Rovira, C.; Veciana, J. *J. Mater. Chem.* **2009**, *19*, 1691.
(97) (a) Minamoto, M.; Matsushita, M. M.; Sugawara, T. *Polyhedron* **2005**, *24*, 2263. (b) Nickels, P.; Matsushita, M. M.; Minamoto, M.; Komiyama, S.; Sugawara, T. *Small* **2008**, *4*, 471. (c) Sugawara, T.; Komatsu, H.; Suzuki, K. *Chem. Soc. Rev.* **2011**, *40*, 3105. (d) Sugawara, T.; Minamoto, M.; Matsushita, M. M.; Nickels, P.; Komiyama, S. *Phys. Rev. B* **2008**, *77*, 235316.
(98) Crivillers, N.; Paradinas, M.; Mas-Torrent, M.; Bromley, S. T.; Rovira, C.; Ocal, C.; Veciana, J. *Chem. Commun.* **2011**, *47*, 4664.
(99) (a) Smeu, M.; DiLabio, G. A. *J. Phys. Chem. C* **2010**, *114*, 17874. (b) Tagami, K.; Tsukada, M. *J. Phys. Chem. B* **2004**, *108*, 6441. (c) Herrmann, C.; Solomon, G. C.; Ratner, M. A. *J. Am. Chem. Soc.* **2010**, *132*, 3682.
(100) (a) Abbott, S.; Ralston, J.; Reynolds, G.; Hayes, R. *Langmuir* **1999**, *15*, 8923. (b) Lahann, J.; Mitragotri, S.; Tran, T. N.; Kaido, H.; Sundaram, J.; Choi, I. S.; Hoffer, S.; Somorjai, G. A.; Langer, R. *Science* **2003**, *299*, 371. (c) Liu, M.; Jiang, L. *Adv. Funct. Mater.* **2010**, *20*, 3753. (d) Wieckowska, A.; Braunschweig, A. B.; Willner, I. *Chem. Commun.* **2007**, 3918. (e) Liu, Y.; Mu, L.; Liu, B. H.; Zhang, S.; Yang, P. Y.; Kong, J. L. *Chem. Commun.* **2004**, 1194.